We would like to thank all our referees for their comments as we appreciate the time dedicated for this review and have made changes to the manuscript to reflect the suggestions. Individual comments from each are bolded with our responses in italics. Attached at the end is our manuscript with changes indicated.

Reviewer 1:

This paper presents a comprehensive evaluation of the TROPOMI satellite NO2 product v1.2 for the New York City/Long Island Sound region, where the NO2 TrVC has high spatial and temporal heterogeneity. The NO2 TrVC measurements from both airborne and ground-based Pandora spectrometers are used to compare with the TROPOMI NO2 products. While Pandora spectrometers provided continuous long-term measurements, airborne spectrometers provide observations with more spatially representative of the satellite measurements. The effects of the cloud retrieval and a priori profile on the biases in TROPOMI NO2 product are analyzed. The study is interesting and provides a welcome addition to the literatures on the measurements of the NO2 TrVCs from satellite, airborne and ground-based spectrometers. The manuscript is well written and the presentation looks good. I would recommend acceptance for publication after the following comments have been addressed.

Specific comments:

What are the exposure time for each scan of GeoTASO and GCAS during the flight and corresponding distance the airplanes flied? I did not find this information in Sect. 2.2.

Integration times for GeoTASO are fixed at 250 ms and GCAS integration times span 225 ms to 750 ms (most the time at 225 ms). I added this information to Table 2. I also added the median aircraft speeds in the text. The ground speed of the HU-25 at altitude averaged 215 m/s, therefore each exposure was ~ 53 m in distance along track. The King Air is slower than the HU-25 with an average ground speed 123 m/s. With the range of integration times, this would mean that one exposure ranged from 30-90 m. Multiple images are co-added to create a pixel size close to 250 m.

The definitions of the tropospheric column seem to be different for satellite (L141-142), airborne (L229-230), and ground-based measurements. In other wards, different 'tropopause altitudes' are used to derive the TrVCs of NO2. Considering that NO2 concentrations in the upper troposphere near the tropopause may be sufficiently large, could these differences in the definition affect the comparisons among the three data sets? How is the airborne stratospheric columns of NO2 retrieved (L268-269)?

Starting with the last question, as another review ask about this this as well. We clarified the airborne spectrometer stratospheric estimation. The airborne stratospheric component is estimated using a stratospheric NO_2 climatology developed using the PRATMO (PRather ATmospheric MOdel) Photochemical Box Model (Prather, 1992; McLinden et al., 2000; Nowlan et al., 2016). The PRATMO column is bias corrected daily using TROPOMI NO_2 stratospheric vertical columns by calculating the average offset between the two datasets over the LISTOS domain for each day (ranging from $5x10^{13}$ to $6x10^{14}$ molecules cm^{-2}). This is stated in Section 2.3. I also avoided calling it stratospheric 'retrieved' as the actual stratospheric vertical column component is

estimated from outside data (TROPOMI+PRATMO) and not directly retrieved but rather that signal is removed when doing the differential slant column to tropospheric vertical column conversion. I added text to Sect. 2.3 to more clearly state this conversion:

> *"Differential slant columns are converted to below aircraft vertical columns (assumed as the tropospheric vertical column, TrVC) by subtracting the estimated stratospheric slant column (climatology bias corrected daily with TROPOMI multiplied by the stratospheric AMF), adding the estimated reference slant column amount (from Pandora) and dividing by the tropospheric air mass factor, similar to Eq. 1 in Judd et al. (2019) or Eq 4. in Nowlan et al. (2018)."*

For each dataset comparisons, we aimed to keep the stratospheric component compatible between the reference and the evaluated measurements. These details are found within the manuscript.

1. *Pandora v. Aircraft: The estimated aircraft stratospheric column is subtracted from Pandora. The uncertainty in that assumed value is in both datasets.*
2. *Pandora v. TROPOMI: For these comparisons, the stratospheric column from the TROPOMI product is subtracted from Pandora. Therefore, that assumption is made in both datasets.*
3. *Aircraft v. TROPOMI: Stratospheric columns retrieved from TROPOMI is part of the estimated airborne column and the largest errors would likely be associated with times furthest from the TROPOMI overpass time as the slope change throughout the day is estimated from the climatology created from PRATMO. So, for airborne/TROPOMI comparisons during the time of the TROPOMI overpass time are mostly comparable. They do use different definitions for the 'tropopause' however, if there were a significant feature making a difference then we would expect to see day-by-day clustering in the comparisons, which we do not. I did go back and calculate what our 'a priori' profile is between the aircraft and the TROPOMI tropopause pressure and that value is less than $2x10^{14}$ molecules cm^{-2} (median is $1.6x10^{14}$ molecules cm^{-2}). We expect any impact to be minimal and would not affect the conclusions made about these comparisons.*

L78-79: In addition to the gradient-smoothing effect, the aerosol-shielding effect may also make a contribution to the uncertainties in the validation of satellite products by ground-based spectrometer, particularly in high-aerosol-load areas (e.g., Ma et al., 2013;Jin et al., 2016). How about the typical aerosol levels over the investigated region? Can the aerosol shielding effect be large enough to affect the comparison of Pandora with TROPOMI and airborne spectrometer measurements?

During Pandora+airborne spectrometer comparisons, over 90% of the coincidences have an AOT at 532 nm < 0.3 (measured by the co-located airborne lidar, HALO), two coincidences are above 0.5 with a max of 0.7. In the supplement, Figure S1 shows the comparison colored by AOT. We added text with the details about AOT during these coincidences to give readers a gauge on aerosol loading. We have also discussed aerosol impacts during outlier coincidences as possible causes during individual cases, though did not find strong evidence that they were a regular impact.

We do not have regular AOT measurements to coincide with the Pandora sites for Pandora/TROPOMI coincidences, therefore we rely on the Pandora algorithm to filter out scenes that are extremely aerosol polluted. In this work, we only use direct-sun measurements, so most of the signal measured by the spectrometer in clear scenes is from the direct solar beam. In the presence of clouds or heavy aerosols, scattered light can become a small fraction of the light observed by the Pandora direct-sun measurement and in the case of heavy aerosol loading (~AOT>1), these measurements are flagged as lower quality (like a cloud). This work only includes high quality measurements, therefore, cases of extreme aerosols are inherently filtered out.

In scenes with lighter aerosol loading, there is the potential for aerosol impacts to the TROPOMI retrieval. In Sect 4.1 we mention that scattering from aerosols are assumed as indirectly sensed through the cloud retrieval, though it is not explicitly accounted for in the TROPOMI retrieval. During aircraft coincidences with TROPOMI,

AOT at 532nm measured by HALO has a mean of 0.22 and a standard deviation of 0.15. This detail been added to Sec. 4.1 for additional context on aerosol loading. In future work, we plan to use aerosol profile measurements from HALO to estimate the sensitivity to aerosol loading in this region, which would enable us to more explicitly answer this question.

For now, we have added the following text to the paper in Sect 7. that references sources promote that aerosol impacts should be included in future investigations

> *"One component not explicitly explored in this work, that should be in the future, is the potential impact of aerosols on the TROPOMI retrieval and whether their indirect accounting through the cloud retrieval accurately reflects the impacts within the radiative transfer calculations for the air mass factor calculation (e.g., Leitão et al., 2010; Ma et al., 2013; Jin et al., 2016)."*

Technical issues:

L21-23: please rephrase the first sentence in the Abstract. It should be stated that

the measurements were made or the measurement data were collected. Better to

describe more clearly which coincided with the early measurements from the Sentinel-

5P TROPOMI instrument?

I reworded the first sentence to say: ' Airborne and ground-based Pandora spectrometer NO_2 column measurements were collected during the 2018 Long Island Sound Tropospheric Ozone Study (LISTOS) in the New York City/Long Island Sound region which coincided with early observations from the Sentinel-5P TROPOMI instrument.'

L37: change 'biggest' to 'largest'.

Change made as requested.

L124: the words 'to be' can be deleted.

I changed the phrase: 'to span late June through..'

L153: how is the qa_value defined?

QA_values are defined within the TROPOMI product file. This is not a value that I am defining. Information on how it is defined is located in the references in this part of the discussion (particularly the product user's manual; Eskes et al., 2019).

L163: what does the dynamic range of NO2 refers to?

The dynamic range is referring to the range of NO_2 columns observed from day to day. This can vary day to day from very clean (less than $1x10^{15}$) to very polluted (up to $100x10^{15}$). The main point in this discussion is that the peak in the annual average in that area is $12x10^{15}$, but day to day variations can be quite a bit more or less polluted than that.

L74: please check the phrase 'through June 30'. Did Hu25 fly only one day?

Table 3 has a summary of the flights and 'through June 30th was referring to all flights prior to and on June 30th. I changed the phrasing to say 'GeoTASO was flown on the NASA LaRC HU-25 Falcon during the three June flight days…'

L187: please give the pressure altitude in hPa.

Instead, I removed the word pressure and refer to it as aircraft indicated altitude, as I am referring to the aircraft being set to fly at an altitude of 28,000 ft according to its altimeter.

L790; 'This is the first work that airborne spectrometer measurement dataset has been used to . . .'?

Changed the sentence to say 'This is the first work that uses an airborne spectrometer dataset to evaluate the TROPOMI tropospheric NO_2 product.'

Figure 2: please add x10^(15) to the labels of both x-axes and y-axes.

This label is on both axes.

References

Ma, J. Z., Beirle, S., Jin, J. L., Shaiganfar, R., Yan, P., and Wagner, T.: Tropospheric NO2 vertical column densities over Beijing: results of the first three years of groundbased MAX-DOAS measurements (2008-2011) and satellite validation, Atmos. Chem. Phys., 13, 1547-1567, 10.5194/acp-13-1547-2013, 2013.

Jin, J., Ma, J., Lin, W., Zhao, H., Shaiganfar, R., Beirle, S., and Wagner, T.: MAXDOAS measurements and satellite validation of tropospheric NO2 and SO2 vertical column densities at a rural site of North China, Atmospheric Environment, 133, 12-25, http://dx.doi.org/10.1016/j.atmosenv.2016.03.031, 2016.

Reviewer 2:

The present manuscript presents the evaluation of S5P TROPOMI tropospheric NO2 column densities with the aid of airborne and ground-based spectrometers in New York City and Long Island Sound. The advantage/ challenge of this region is that the NO2 concentrations are highly heterogeneous in time and space. The validation of S5P TROPOMI tropospheric NO2 column densities is separated in two major categories: (1) comparison between airborne NO2 TrVC and TROPOMI NO2 TrVC and (2) comparison between ground-based NO2 TrVC and TROPOMI NO2 TrVC. From the abovementioned comparisons, the authors observe a bias in TROPOMI NO2 TrVC and the effect of clouds and a-priori profile in the TROPOMI retrieval are examined into details. I strongly recommend the publication of the manuscript after consideration of a minor number of specific considerations:

Specific comments:
– Page 2, Line 60: It would be interesting to add the exact spatial resolution of OMI and OMPS.
Spatial resolutions were added to this discussion.

– Page 4, Line 110: I suggest that for the reader it would be more practical if you include a small separate section or subsection called "LISTOS campaign" and write

there the information about the campaign, as you already did in Section 2.
The first paragraph in Section 2 serves this purpose as the campaign description. I added a subsection header to this paragraph so that a reader can easily identify where the campaign information is discussed.

– Page 7, Line 218: Please explain the PRATMO acronym
In other sources that cite this model, PRATMO is not defined as an acronym. However, we did find out it is short for 'Prather Atmospheric Model'. I defined this in the text.

– Page 8, Line 234: If I understand well, did you assume that the aerosol a-priori profile in the AMF calculation is zero? So, you assumed that no aerosols are present in the atmosphere, or not? If this the case, is this assumption leading to realistic results?
You understood the assumption correctly that aerosol a priori profile is zero for this analysis. However, as shown by our comparison to Pandora, in which the direct-sun measurements are largely insensitive to aerosols at the levels observed, we still compare really well so we expect impacts due to aerosols to be smaller than the other sources of bias we have found in this analysis. However, in future work, we plan to incorporate the HALO aerosol profile data into our retrieval to directly assess potential impacts.

– Page 18, Line 580: Can you provide an approximate value for the Pandora horizontal sensitivity?

Pandora's approximate horizontal path through the lower troposphere where most of the NO2 resides is quite small and local (less than 1 km). For example, if we had a 1km mixed layer height and the range of SZAs during the LISTOS time period (17-40 degrees), the horizontal pathlength through the mixed layer would range from ~300-840 m.

In reference to the horizontal bars in the figure mentioned (Figure 10), which is where I originally thought the comment was referring to, the temporal variation in Pandora is proportional to pollution level (10^{th}-90^{th} percentile range vs. Pandora TrVC: r^2=0.69 and y(range)=0.47(TrVC)-0.52x10^{15} molecules cm^{-2}). I added the following sentence to the text: 'Temporal variation of TrVCs measured by Pandora increases proportionally to pollution level (r^2=0.69).'

– Page 19, Line 581: This means that the Pandora data are not filtered for clouds?
I think you are referring to the phrase 'Although cloud information for Pandora comparisons at TROPOMI sub-pixel resolution is not readily available…' does make it sound like Pandora data were not cloud filtered but this is not the case. Clouds are filtered in Pandora algorithm through their quality flags. The intention was that Pandora has the ability to still have a clear direct line of the sun even if TROPOMI has broken clouds (elevated cloud fractions), but we don't have direct measurements of sub-pixel cloud coverage like we do from the airborne spectrometer data.

I changed this sentence to be clearer: 'Unlike with airborne spectrometer data, sub-TROPOMI pixel cloud information is not readily available for these comparisons to Pandora. However, the impact of coincidence criteria…'

– Page 21, Line 650: Is there a reason why you did not compare Pandora TrVC (vs) TROPOMI-NAMCMAQ for the extended time period? I would be interesting to add a figure with this comparison.
The NAMCMAQ runs that we used are only available through September 2018 as they were run as part of the LISTOS campaign and not operationally. Future work in this area (as many of these Pandoras will operate over a longer time period in this region) will consider sources for higher resolution a priori data available over a longer time period (e.g., the NASA GEOS-CF at 25 km resolution) and assess the impact to the results.

– Page 21, Line 678: You could cite studies that use MAX-DOAS measurements to evaluate the TROPOMI NO2 product.
I added studies using the MAX-DOAS technique to evaluate TROPOMI NO2. Though it is noted 1 has been accepted but not available yet (Chan), and the final two are still in discussion in AMTD. .

Chan, K. L., Wiegner, M., Alberti, C., and Wenig, M.: MAX-DOAS measurements of tropospheric NO_2 and HCHO in Munich and the comparison to OMI and TROPOMI satellite observations, Atmos. Meas. Tech. Discuss., https://doi.org/10.5194/amt-2020-35, in review, 2020.

Liu, M., Lin, J., Kong, H., Boersma, K. F., Eskes, H., Kanaya, Y., He, Q., Tian, X., Qin, K., Xie, P., Spurr, R., Ni, R., Yan, Y., Weng, H., and Wang, J.: A new TROPOMI product for tropospheric NO_2 columns over East Asia with explicit aerosol corrections, Atmos. Meas. Tech., 13, 4247–4259, https://doi.org/10.5194/amt-13-4247-2020, 2020.

Dimitropoulou, E., Hendrick, F., Pinardi, G., Friedrich, M. M., Merlaud, A., Tack, F., De Longueville, H., Fayt, C., Hermans, C., Laffineur, Q., Fierens, F., and Van Roozendael, M.: Validation of TROPOMI tropospheric NO_2 columns using dual-scan MAX-DOAS measurements in Uccle, Brussels, Atmos. Meas. Tech. Discuss., https://doi.org/10.5194/amt-2020-33, in review, 2020.

Verhoelst, T., Compernolle, S., Pinardi, G., Lambert, J.-C., Eskes, H. J., Eichmann, K.-U., Fjæraa, A. M., Granville, J., Niemeijer, S., Cede, A., Tiefengraber, M., Hendrick, F., Pazmiño, A., Bais, A., Bazureau, A., Boersma, K. F., Bognar, K., Dehn, A., Donner, S., Elokhov, A., Gebetsberger, M., Goutail, F., Grutter de la Mora, M., Gruzdev, A., Gratsea, M., Hansen, G. H., Irie, H., Jepsen, N., Kanaya, Y., Karagkiozidis, D., Kivi, R., Kreher, K., Levelt, P. F., Liu, C., Müller, M., Navarro Comas, M., Piters, A. J. M., Pommereau, J.-P., Portafaix, T., Puentedura, O., Querel, R., Remmers, J., Richter, A., Rimmer, J., Rivera Cárdenas, C., Saavedra de Miguel, L., Sinyakov, V. P., Strong, K., Van Roozendael, M., Veefkind, J. P., Wagner, T., Wittrock, F., Yela González, M., and Zehner, C.: Ground-based validation of the Copernicus Sentinel-5p TROPOMI NO_2 measurements with the NDACC ZSL-DOAS, MAX-DOAS and Pandonia global networks, Atmos. Meas. Tech. Discuss., https://doi.org/10.5194/amt-2020-119, in review, 2020.

– Page 22, Line 699: Please add some reference studies.
A couple references were added to the text in reference to this line.

– Page 39, Table 5: Is there a reason why you did not present the median percentage difference for the Standard Slant Column?
I may have had a reason initially, which was likely because it was a slant column comparison and we don't expect them to be comparable, however, I added the statistics just to be consistent since I do report the linear fits (which demonstrates how correlated the two datasets are).

– Page 46, Figure 6: I would suggest that in Fig. 6a, you include the reported TROPOMI SCD error.
*There is not a reported tropospheric SCD precision in the product file. However, I did look into calculating an uncertainty for tropospheric slant column by considering the slant column equivalent of the first two terms in equation 22 in the ATBD (*http://www.tropomi.eu/sites/default/files/files/publicS5P-KNMI-L2-0005-RP-ATBD_NO2_data_products-20190206_v140.pdf*) and the value is small enough that the vertical error bars are not visible in Figure 6a. The mean is 5.5x10^{14} molecules cm^{-2} with a standard deviation of 7.4x10^{13} molecules cm^{-2}. In the figure caption, I added a statement about this.*

– Page 47, Figure 7: The figure does not contain error bars in the vertical axis. Is there any way to estimate the TROPOMI-NAMCMAQ error and add it to the figure?
We do not have an estimate of TROPOMI-NAMCMAQ error.

Reviewer 3:

This paper by Judd et al. compares satellite-based TROPOMI tropospheric NO_2 measurements with airborne- and ground-based Pandora measurements in the New-York City/Long Island Sound region. It contributes to the Sentinel-5P TROPOMI validation and is the first validation paper for the new satellite instrument with airborne campaign measurements which have a more spatially representativity than ground-based measurements. In addition, long-terme ground-based Pandora measurements are used and compared to the airborne and satellite based NO_2 measurements. The strength of

both reference measurements are used to evaluate TROPOMI tropospheric NO_2 column densities. The evaluation found a low bias of the TROPOMI tropospheric vertical column (TrVC) compared to Pandora and aircraft tropospheric vertical column, more pronounced for aircraft than Pandora measurements. Although using a higher resolution a priori vertical profile for the TROPOMI data improves the low bias, there is still a low bias, especially for more polluted cases and further investigations are needed in future studies.
Cloud retrieval effects are discussed. A new quality criterion was introduced which excludes pixel where the difference between retrieved cloud pressure and surface pressure exceeds 50 hPa to exclude pixels where cloud shielding occurred over cloud free scenes. These pixels compensate partially for the TROPOMI TrVC low bias but lower the correlations with reference measurements.
The paper is well written and of significance for the validation of the new satellite Sentinel-5P TROPOMI tropospheric NO_2 measurements. Therefore, I recommend publication in AMT with minor revisions.

Specific comments:
Line 197: "All reference spectra were co-located with total column NO_2 measurements from Pandora spectrometers: $5.6*10^{15}$ molecules cm^{-2} at MadisonCT on June 30th, $5.7*10^{15}$ molecules cm^{-2} at MadisonCT on July 2nd, and $6.2*10^{15}$ molecules cm^{-2} at WestportCT on August 5th, with values estimated to be over 50% stratospheric."
What is done with the collocated Pandora measurements? How is the 50% stratospheric estimated?
The Pandora measurements are collected during co-located reference spectra scenes by the airborne spectrometer and are used to estimate the total column for our reference. The airborne spectrometer NO2 data has its own above aircraft (stratospheric) value estimated based on coincident TROPOMI stratospheric columns with the diurnal pattern from a climatology created with the PRATMO photochemical box model. That separation is needed in the calculation converting differential slant column to vertical column (e.g., the screenshot equation from Lamsal et al., 2017) with various other versions found in Judd et al, (2019) and Nowlan et al. (2018). I also added some text to reflect this calculation in Sect 2.3.

$$\Omega_v\downarrow = \frac{d\Omega_s - \Omega_v\uparrow \times A\uparrow + \left(\Omega_v{}^R\downarrow \times A^R\downarrow + \Omega_v{}^R\uparrow \times A^R\uparrow\right)}{A\downarrow}.$$

They are estimated as 50% by using the estimated airborne stratospheric column.

$$\Omega_{Pandora\ troposphere} = \Omega_{Pandora} - \Omega_{airborne\ stratosphere}$$
$$\text{where } \Omega_{Pandora\ troposphere} = \Omega_v^R \Downarrow \quad and\ \Omega_{airborne\ stratosphere} = \Omega_v^R \Uparrow$$

Line 292: What is the spatial coincidence criterion for Pandora comparisons to TROPOMI? Is it the nearest pixel, a mean, is the viewing direction considered?
It is the pixel in which the Pandora resides and viewing direction is not considered. This is clarified in Sect. 2.5.

Line 254: "All Pandora data are converted from total vertical columns to TrVCs by subtracting either the airborne or TROPOMI retrieved stratospheric columns for comparison purposes."
Is the Pandora converted with TROPOMI retrieved stratospheric column used for TROPOMI comparisons and Pandora converted with airborne for airborne comparisons?
Yes and yes.
How is the airborne stratospheric column retrieved?
The airborne stratospheric component is estimated using a stratospheric NO_2 climatology developed using the PRATMO (PRather ATmospheric MOdel) Photochemical Box Model (Prather, 1992; McLinden et al., 2000; Nowlan et al., 2016). The stratospheric column is bias corrected daily using TROPOMI NO_2 stratospheric vertical columns by calculating the average offset between the two datasets over the LISTOS domain for each day (ranging from $5x10^{13}$ to $6x10^{14}$ molecules cm^{-2}). To reflect this I reworded the sentence to say: 'All Pandora data are converted from total vertical columns to TrVCs by subtracting either the airborne estimated or TROPOMI retrieved stratospheric columns for comparison purposes.'

Line 450: Why was this feature only seen by this excluded Pandora?

It is by the nature of the plume, which is stated in Section 4, which we did observe with the airborne spectrometer. See below for an image of the large change in morning and afternoon and the structure of the plume intercepted by CCNY. The time difference between the morning and afternoon flight is larger than TROPOMI temporal window (a few hours), however the difference captured in the extreme pollution in this plume is still reflected (note log10 color scale).

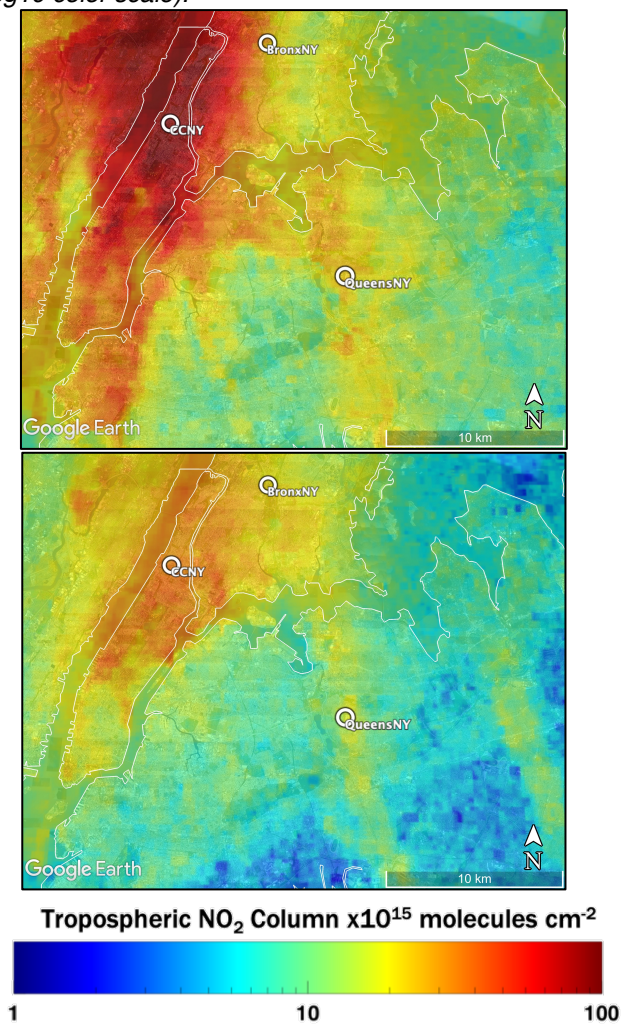

Airborne spectrometer NO2 TrVC during the morning (top) and afternoon (bottom) flights of July 2nd, 2018. The labeled circles indicate 3 Pandora locations, where CCNY is not included in this analysis (will be investigated for future work).

Line 571: Is there an explanation why the slope is much better and the correlation much worse when comparing TROPOMI and Pandora instead of TROPOMI and aircraft measurements?

The correlation is better for the airborne spectrometer because the TROPOMI sub-pixel variation is sampled by the airborne data. However, Pandora data is still subject to impacts from sub-pixel variability in this heterogeneous environment. It seems to be that the slope of the fit is also related to the sub-pixel heterogeneity. If you look at Table 6, you'll note that for sites where r^2 is greater than 0.5, the slopes range from 0.53 to 0.84.

Line 675: Lorente et al. did not used Pandora spectrometers for validation, they also found a low bias but with in-situ measurements.
You are right, the wording was wrongly reflecting Lorente et al. since they use in situ data. I broadened the scope of this paragraph now to include some other studies (including MAX-DOAS observational studies) as suggested by another reviewer.

Technical corrections:
Line 99: LISTOS is defined and used already in line 21 and 36.
I removed this definition of LISTOS. Now it should only be defined once in the abstract and once in the main manuscript.

Line 283: "TROPOMI NO_2 columns"
Better TrVC to be consistent to the other TrVCs in the sentence.
I see this point. However, during editing, this sentence had already changed in the next version and doesn't have this discrepancy anymore.

Line 372: "(Table S1, compare Row I to Row B) slightly improves the correlation (r_2 increases from 0.93 to 0.94)"
Row I is 0.94 and row B 0.92. Value 0.93 should be changed to 0.92 and order of "compare Row I to Row B" should be changed to "B to I" to make it consistent to the values order.
Thanks for catching the translation error in the r^2. This was fixed.

Line 420: "with large sub-pixel variation as indicated by the horizontal whiskers in the plot" There is a better explanation but some lines later (Line 433). This one could be replaced by the later one.
"The horizontal bars in Fig. 6 show the standard deviation of the subpixel airborne TrVCs within each TROPOMI pixel."
I removed the former phrase opting for the later discussion of spatial variation.

Line 556/Figure 9: Statistics are only listed in the table. It would be helpful for a better reading to have at least the statistics of the LISTOS time period data in the figure especially because these are much more discussed in the following than the statistics of the long-term TROPOMI-Pandora comparison.
I added the statistics for the LISTOS time period to Figure 9.

Line 651: r_2 of 0.89 should be 0.88 corresponding to the figure.
Updated the figure. R^2 is 0.885, which rounds up to 0.89. Thanks for catching this error in translation.

Line 714: r_2 of 0.84 should be 0.88
It should be 0.84 as I am referring to only the LISTOS timeframe for all Pandora sites (Figure 10a).

Line 722: and
corrected

Table 2: kg instead of lbs
Converted the weights to kg.

Table 3: Short explanation for shaded boxes
Added: 'Flights with shaded boxes are not considered in this analysis.' to the table description. Explanation is in the text as to why they aren't include: 'Only flights from 25 June – 6 September (13 flight days) are considered in this analysis due to availability of the high-resolution model data used to provide the a priori NO_2 profile shapes in the full vertical column retrieval (Table 1)'

Figure 1: Nine Pandora spectrometers instead of spectrometer.

Fixed

Figure 2: Explanation to horizontal and vertical bars with "variability at the time of measurement" is missing in figure caption.
For brevity it is described by the '(± min/max observation within a ± 5-minute window from the aircraft overpass)' and '(±10th-90th percentile)'.

Figure 10: The period (LISTOS or extended long-term) of the used data is missing.
Good catch! Added this detail.

Figure 12: (a) Also for the LISTOS comparison only the extended stations are used
I clarified this figure caption now to ensure it states that it is only the four stations with extended temporal extent.

Supplement Line 53: "to remove the estimated of loss of sensitivity"
First "of" can be removed
This phrase was corrected.

Other changes made in addition to reviewer suggestions:

1. *In the supplement, the color bar in Figure S1 was reversed. This has been fixed.*
2. *It also came to light that we had an error in information about the Pandora located at CCNY where the data file stated the altitude of the instrument was 113 meters, while it is 113 ft (or approx. 30 meters) above the ground level. Notes about this detail have been removed from the Pandora section as they were inaccurate (and should be fixed in the data file). In the end, speaking with the instrument Principal Investigator and operator, Maria Tzortziou at CCNY, we opted to not include data from this instrument into the quantitative analysis and kept it to PAMS-EM sites as originally done. These types of comparisons at CCNY will be investigated further in future work with the hopes of also linking the measurements to some other observations in NYC, including a boat-based Pandora in Long Island Sound.*

Tracked changes to the manuscript and its supplement can be seen below.

Evaluating Sentinel-5P TROPOMI tropospheric NO_2 column densities with airborne and Pandora spectrometers near New York City and Long Island Sound

Laura M. Judd[1], Jassim A. Al-Saadi[1], James J. Szykman[2], Lukas C. Valin[2], Scott J. Janz[3], Matthew G. Kowalewski[3,4], Henk J. Eskes[5], J. Pepijn Veefkind[5,6], Alexander Cede[7], Moritz Mueller[7], Manuel Gebetsberger[7], Robert Swap[3], R. Bradley Pierce[8], Caroline R. Nowlan[9], Gonzalo González Abad[9], Amin Nehrir[1], David Williams[2]

[1]NASA Langley Research Center, Hampton, VA, 23681, United States
[2]United States Environmental Protection Agency Office of Research and Development, Triangle Research Park, NC, 27709, United States
[3]NASA Goddard Space Flight Center, Greenbelt, MD, 20771, United States
[4]Universities Space Research Association, Columbia, MD, 21046, United States
[5]Royal Netherlands Meteorological Institute (KNMI), De Bilt, Netherlands
[6]Delft University of Technology, Department of Geoscience and Remote Sensing, Delft, Netherlands
[7]LuftBlick, Kreith, Austria
[8] University of Wisconsin-Madison Space Science and Engineering Center, Madison, WI, 53706, United States
[9]Harvard-Smithsonian Center for Astrophysics Cambridge, MA, 02138

Correspondence to: Laura M. Judd (laura.m.judd@nasa.gov)

Abstract. Airborne and ground-based Pandora spectrometer NO_2 column measurements were collected during the 2018 Long Island Sound Tropospheric Ozone Study (LISTOS) in the New York City/Long Island Sound region which coincided with early observations from the Sentinel-5P TROPOMI instrument. Both airborne- and ground-based measurements are used to evaluate the TROPOspheric Monitoring Instrument (TROPOMI) NO_2 Tropospheric Vertical Column (TrVC) product v1.2 in this region, which has high spatial and temporal heterogeneity in NO_2. First, airborne and Pandora TrVCs are compared to evaluate the uncertainty of the airborne TrVC and establish the spatial representativeness of the Pandora observations. The 171 coincidences between Pandora and airborne TrVCs are found to be highly correlated (r^2=0.92 and slope of 1.03) with the largest individual differences being associated with high temporal and/or spatial variability. These reference measurements (Pandora and airborne) are complementary with respect to temporal coverage and spatial representivity. Pandora spectrometers can provide continuous long-term measurements but may lack areal representivity when operated in direct-sun mode. Airborne spectrometers are typically only deployed for short periods of time, but their observations are more spatially representative of the satellite measurements with the added capability of retrieving at subpixel resolutions of 250 m × 250 m over the entire TROPOMI pixels they overfly. Thus, airborne data are more correlated with TROPOMI measurements (r^2=0.96) than Pandora measurements are with TROPOMI (r^2=0.84). The largest outliers between TROPOMI and the reference measurements are caused by errors in the TROPOMI retrieval of cloud pressure impacting the calculation of tropospheric air mass factors in cloud-free scenes. This factor causes a high bias in TROPOMI TrVCs of 4-11%. Excluding these cloud-impacted points,

Deleted: Abundant NO_2 column measurements from
Deleted: a
Deleted: s
Deleted: as part of the
Deleted: and
Deleted: measurements
Deleted: biggest

TROPOMI has an overall low bias of 19-33% during the LISTOS timeframe of June-September 2018. Part of this low bias is caused by coarse a priori profile input from TM5-MP model; replacing these profiles with those from a 12km NAMCMAQ analysis results in a 12-14% increase in the TrVCs. Even with this improvement, the TROPOMI-NAMCMAQ TrVCs have a 7-19% low bias, indicating needed improvement in a priori assumptions in the air mass factor calculation. Future work should explore additional impacts of a priori inputs to further assess the remaining low biases in TROPOMI using these datasets.

1 Introduction

Nitrogen dioxide (NO_2) is an air pollutant emitted naturally through soil emissions and lightning, and anthropogenically as a combustion product from sources such as mobile vehicles, powerplants, and industrial processes. NO_2 is harmful to human health (e.g., Fischer et al., 2015; Anenberg et al., 2018) both directly and through its role in the production of near-surface ozone and particulate matter making it a criteria air pollutant monitored and regulated by the Clean Air Act (https://www.epa.gov/clean-air-act-overview: last accessed 18 April 2020). Due to its short lifetime of a few hours as a component of NOx ($NO + NO_2$) (Liang et al., 1998; Beirle et al., 2011; Liu et al., 2016), the spatial distribution of NO_2 near anthropogenic emission sources is highly heterogeneous with complex patterns that are hard to characterize from sparse networks of ground-based monitors.

The TROPOspheric Monitoring Instrument (TROPOMI) on board the Copernicus Sentinel-5 Precursor (S5P) satellite currently measures column densities of NO_2 globally at unprecedented spatial resolution making it an important tool for studying and monitoring urban air pollution. TROPOMI continues a long legacy of UltraViolet-VISible (UV-VIS) backscatter measurements from satellites observing trace gas column densities related to air quality (González Abad et al., 2019). Global NO_2 measurements have heritage from the Global Ozone Monitoring Experiment (GOME; Burrows et al., 1999), SCanning Imaging Absorption SpectroMeter for Atmospheric CHartographY (SCIAMACHY; Bovensmann et al., 1999), GOME-2 (Callies et al., 2000; Behrens et al., 2018), Ozone Monitoring Instrument (OMI; Levelt et al., 2006; Levelt et al., 2018), Ozone Mapping and Profiling Suite (OMPS; Yang et al., 2014), and as of October 2017, TROPOMI (Veefkind et al., 2012) aboard S5P. Over the last couple decades, the spatial and temporal resolution of these satellite NO_2 products have improved with the first daily global coverage achieved by OMI launched in 2004 and with TROPOMI achieving a spatial resolution an order of magnitude finer (currently approximately 3.5 km × 5.5 km at nadir) than the still-operating OMI (13 km x 24 km at nadir) and OMPS (50 km x 50 km at nadir on Suomi-NPP) instruments.

The use of the TROPOMI tropospheric NO_2 products for applications such as evaluating emissions inventories and distinguishing point sources has already been documented in recent literature. Goldberg et al. (2019) used data from the first year of TROPOMI operation to evaluate top-down NOx emissions over three major U.S. cities and two large powerplants. Complementary studies also pinpointed emissions from large point sources (Beirle et al., 2019) and even showed that emissions in Paris, France, have not decreased as expected since 2012 (Lorente et al., 2019). Griffin et al. (2018) found that the improved

spatial resolution of TROPOMI was able to distinguish NO_2 plumes from individual sources near the Canadian Oil Sands, which was not possible with the coarser measurements from OMI.

To enhance the integrity of using TROPOMI data in research and applications, each product requires systematic evaluation and validation. Validation activities include evaluating the data products under polluted and clean scenes using reference measurements from satellite, airborne, and ground-based instrumentation (van Geffen et al., 2019). Routine TROPOMI NO_2 validation reports are produced regularly and documented at http://mpc-vdaf.tropomi.eu/ (last accessed: 30 March 2020). Additional in-depth studies in recent literature have been mostly confined to ground-based column measurements from MAX-DOAS and/or direct-sun column measurements (e.g., from Pandora spectrometers) (e.g., Griffin et al., 2018, Zhao et al., 2019, Ialongo et al., 2020, Wang et al., 2020). These types of measurements have been used in the past to evaluate the OMI Tropospheric Vertical Column (TrVC) product, though this was shown to be challenging in polluted areas as spatial variability in NO_2 can result in sampling mismatches between the small spatial scale measurements from the ground-based spectrometers and the > 300 km^2 pixels from OMI (Lamsal et al., 2014; Reed et al., 2015; Goldberg et al., 2017; Judd et al., 2019). Initial results of TROPOMI NO_2 product validation with Pandora spectrometer direct-sun measurements show more encouraging results with higher levels of correlation than OMI evaluations (OMI examples found in Goldberg et al., 2017 and Judd et al., 2019; TROPOMI examples found in Griffin et al., 2018, Zhao et al., 2019, Ialongo et al., 2020, and this work).

In addition to ground-based column measurements, airborne column mapping datasets have been identified as valuable for TROPOMI TrVC validation efforts (van Geffen et al., 2019). Airborne spectrometers have the capability to map at much finer spatial resolutions than current satellite-based observations; for example, those used in this study have a spatial resolution of approximately 250 m × 250 m. Airborne spectrometers have been used to visualize high spatiotemporal variations in NO_2 over select areas in Europe, North America, Africa, and Asia (Popp et al., 2012; Schönhardt et al., 2015; Lawrence et al., 2015; Nowlan et al., 2016, 2018; Lamsal et al., 2017; Meier et al., 2017; Tack et al., 2017, 2019, Broccardo et al., 2018; Judd et al., 2018, 2019) and have even contributed toward evaluating emissions inventories and ozone production sensitivity (Schönhardt et al., 2015; Souri et al., 2018; Souri et al., 2020). Measurements from airborne spectrometers have also been compared to the OMI NO_2 products. Broccardo et al. (2018) found that agreement between the airborne mapper, iDOAS, and OMI improves with distance away from large emission source regions. Lamsal et al. (2017) discovered moderate correlation during a small subset of comparisons between the Airborne Compact Atmospheric Mapper (ACAM) and OMI over the Maryland region in 2011, though large differences were found for instances with insufficient sampling by the airborne mapper in areas subject to spatial heterogeneity of NO_2. The large pixels from OMI are difficult to completely sample with airborne spectrometer observations; however, with the improved spatial resolution of TROPOMI, representative sampling by airborne spectrometers is less of a concern as will be demonstrated in this work.

In this study, we use data from two NASA airborne spectrometers and nine ground-based (Pandora) spectrometers to evaluate the S5P TROPOMI NO_2 TrVC v1.2 product over New York City (NYC) and Long Island Sound during the summer 2018 LISTOS field campaign. The intercomparisons between the three independent datasets help bound NO_2 product uncertainties due to spatial and temporal variability and a priori assumptions within the retrievals. Section 2 introduces

Deleted: Long Island Sound Tropospheric Ozone Study (

Deleted:)

LISTOS and each NO_2 dataset: S5P TROPOMI, the airborne spectrometers, and Pandora spectrometer, along with details on methodology. Section 3 evaluates the airborne spectrometer retrieval using Pandora measurements. Section 4 presents comparisons of TROPOMI NO_2 columns to the airborne spectrometer observations during LISTOS. Section 5 compares TROPOMI NO_2 TrVCs to Pandora spectrometer data for the LISTOS timeframe as well as expanded through winter 2019. Throughout these sections causes for bias in the TROPOMI product based on the a priori profile and cloud assumptions are discussed. Section 6 summarizes TROPOMI NO_2 TrVC performance in the NYC region and Sect. 7 presents concluding remarks. Together these results demonstrate TROPOMI's capability for observing the spatial distribution of NO_2 in heterogeneous environments and demonstrate approaches for resolving apparent differences associated with linking observations from different measurement strategies.

2 Data and Methods

2.1 The Long Island Sound Tropospheric Ozone Study

Data in this study were acquired across the NYC and Long Island Sound region in the United States as part of the Long Island Sound Tropospheric Ozone Study (LISTOS: https://www.nescaum.org/documents/listos; https://www-air.larc.nasa.gov/missions/listos/index.html : last accessed 18 April 2020). LISTOS was a multi-organizational collaborative air quality study focused on understanding the sources and temporal emission profiles of the ozone precursors, nitrogen oxides (NOx) and volatile organic compounds (VOCs), across the NYC metropolitan area and ozone formation and transport in this coastal region. Measurements conducted include in situ and remotely sensed air quality and meteorology measurements from satellites, aircraft, and ground sites as well as the integration of the measurements with air quality models. This urban to sub-urban coastal area is a diverse region for validating satellite products due to the heterogeneous patterns in pollution as well as varying environmental factors such as surface reflectivity. In this study, we consider measurements from the LISTOS timeframe to span late June through September 2018, though some measurements extended before and after this time period.

Deleted: be

Deleted: from

Deleted: 1

2.2 S5P TROPOMI

Sentinel-5 Precursor (S5P) was launched October 2017 into a sun-synchronous low Earth orbit with a 13:30 local equator crossing time. S5P carries a single instrument, TROPOMI, which consists of a hyperspectral spectrometer observing eight bands spanning the ultraviolet (UV), visible (VIS), near infrared, and shortwave infrared portions of the electromagnetic spectrum (Veefkind et al., 2012). The S5P orbit combined with the wide TROPOMI swath width of 2600 km provide observations between approximately 17:00-19:00 UTC (13:00-15:00 EDT) over the New York City and Long Island Sound region, capturing the early afternoon spatial distribution of trace gas columns including CO (Borsdorff et al., 2018), HCHO (De Smedt et al., 2018), CH_4 (Hu et al., 2017), NO_2 (van Geffen et al., 2019 & 2020), SO_2 (Theys et al., 2017), and O_3 (Garane et al., 2019).

In this work, the TROPOMI v1.2 NO_2 TrVC product is evaluated with airborne and ground-based column density measurements from 25 June 2018 - 19 March 2019 over the LISTOS domain. The retrieval is built on the heritage of the Ozone Monitoring Instrument DOMINO product (Boersma et al., 2011) including developments from the QA4ECV project (Boersma et al., 2018; van Geffen et al., 2019; http://www.qa4ecv.eu/: last accessed 18 April 2020). NO_2 total slant columns are retrieved via the Differential Optical Absorption Spectroscopy (DOAS; Platt and Stutz, 2008) method in the visible window of 405-465 nm. Following the spectral fit, the slant columns are separated into their stratospheric and tropospheric components. The stratospheric column is estimated by assimilating the total columns in the TM5-MP model. The remaining tropospheric slant columns are converted into vertical columns through the calculation and application of air mass factors (AMFs; Palmer et al., 2001). A priori inputs for the tropospheric NO_2 AMF calculations include viewing and solar geometry, surface pressure and NO_2 profile shape from the 1° × 1° TM5-MP model (Williams et al. 2017), 0.5° × 0.5° surface albedo climatology built upon 5 years of OMI data (Kleipool et al. 2008), and the FRESCO-S cloud fraction and cloud height (Loyola et al., 2018) (Table 1).

TROPOMI data during the time period of this analysis have a nadir spatial resolution of 3.5 km × 7 km, with pixel areas ranging from 32.5 - 129.5 km^2. Beginning on 6 August 2019, the nadir spatial resolution of the TROPOMI NO_2 product is refined to 3.5 km × 5.5 km (Ludewig et al., 2020). TROPOMI is capable of observing pollution at a spatial resolution a factor of 10 times more refined than its predecessor satellite sensor, OMI (Levelt et al., 2006; Levelt et al., 2018).

Only TROPOMI data with qa_value = 1 are considered in this analysis, which removes pixels influenced by issues such as sun glint, missing retrieval information, or cloud radiative fractions (CRF) above 50% (van Geffen et al., 2019, Eskes et al., 2019). We note that qa_values down to 0.75 are deemed acceptable for most data uses but 2% or less of the TROPOMI data in this work had qa_values between 0.75 and 1 and do not affect the results. This work also makes use of the averaging kernel and pressure profiles used in the retrieval to explore the impact of different NO_2 profile shapes within the air mass factor calculation and explores sensitivity of the results to cloud retrievals during clear-sky scenes.

Figure 1 shows the annual average of NO_2 TrVCs observed over the LISTOS region from April 2018-March 2019, depicting peak NO_2 in the domain of over 10×10^{15} molecules cm^{-2} over much of New York City. The largest value is over the southern tip of Manhattan Island at a magnitude of 12×10^{15} molecules cm^{-2}. The spatial distribution and dynamic range of NO_2 varies widely day-to-day over this region due to variable meteorology, emissions, and the lifetime of NO_2, as shown through examples in this analysis.

2.3 Airborne Spectrometers

Deleted: 2

Two airborne UV-VIS mapping spectrometers are used in this study: Geostationary Trace gas and Aerosol Sensor Optimization (GeoTASO) and GEO-CAPE Airborne Simulator (GCAS). GeoTASO and GCAS are very similar instruments but differ in characteristics such as their size, weight, wavelength range, and sensitivity. Specific details about these two instruments can be found in Leitch et al. (2014), Kowalewski and Janz (2014), Nowlan et al. (2016), and Nowlan et al. (2018) with a brief

summary in Table 2. The two instruments have very similar performance with respect to the NO_2 retrieval. Due to varying aircraft availability during LISTOS, these instruments were flown either interchangeably or together during 16 flight days between 18 June 2018 – 19 October 2018. Only flights from 25 June – 6 September (13 flight days) are considered in this analysis due to availability of the high-resolution model data used to provide the a priori NO_2 profile shapes in the full vertical column retrieval (Table 1). GeoTASO was flown on the NASA LaRC HU-25 Falcon during the three June flight days and GCAS was flown on the NASA LaRC B200 from July through October. The HU-25 Falcon is a faster aircraft (average ground speed at altitude was 215 m s^{-1}) capable of mapping approximately a 50% larger area per flight than the B200 (average ground speed at altitude was 123 m s^{-1}). This capability enabled us to also conduct measurements for the second Ozone Water-Land Environmental Transition Study domain (OWLETS2: https://www-air.larc.nasa.gov/missions/owlets/index.html: last accessed 7 January 2020) during June flights over Baltimore, Maryland in the early morning and late afternoon hours (outside the S5P overpass window). The NASA LaRC B200 has two nadir-viewing remote sensing portals, allowing installation of a second instrument along with GCAS. The second instrument from July through September was the High Altitude Lidar Observatory (HALO: Nehrir et al. 2019) providing co-located measurements of nadir profiles of aerosols and methane. This analysis uses HALO aerosol optical thickness (AOT) retrievals at 532 nm to discuss aerosol conditions qualitatively. GeoTASO was the second instrument for flights in October, allowing for direct comparison of GCAS and GeoTASO retrievals, however these flights did not coincide with any clear-sky TROPOMI overpasses.

Figure 1 shows the two basic "raster" patterns that were flown by the NASA aircraft to create gapless maps of the high spatial resolution spectra from which NO_2 TrVCs are retrieved. Both airborne instruments have a swath width of approximately 7 km at the nominal flight altitude of 9 km (aircraft indicated altitude of 28,000 ft), thus flight lines are spaced slightly over 6 km apart to ensure overlap between adjacent swaths. Table 3 includes a summary of all flights considered in this study along with cloud conditions, number of coincidences with Pandora and TROPOMI (assuming coincidence criteria discussed in Sect. 2.5 and throughout this manuscript), and raster type. All flight days included two flights lasting approximately 4-5 hours each (morning and afternoon). The small raster (white lines in Fig. 1) could be accomplished 2 times in one flight (4 times per day), repeatedly measuring the same area to observe the temporal variation throughout the day. The large raster (black lines in Fig. 1) could only be flown once per flight (twice per day) and was meant to capture a more regional view of the spatial distribution of NO_2 on days with expected air pollution over Long Island Sound and the surrounding communities.

The NO_2 retrieval algorithm is identical for GCAS and GeoTASO. The retrieval process is summarized here with additional detail in Judd et al. (2019). NO_2 differential slant columns are retrieved at an approximate spatial resolution of 250 m × 250 m in the spectral fitting window of 425-460 nm relative to an in-flight measured reference spectra using the open-source DOAS computing software, QDOAS (http://uv-vis.aeronomie.be/software/QDOAS/; last accessed 18 April 2020). Reference spectra were collected over areas with low and homogeneous NO_2 absorption over a 4-5-minute time period using nadir observations for each of the 30 across-track positions. Three separate references were collected during the LISTOS campaign: June 30th for all GeoTASO flights, July 2nd for the GCAS flights for this day only (due to unique instrument

Deleted: through
Deleted: June 30th
Deleted: September
Formatted: Superscript
Formatted: Superscript
Deleted: pressure
Deleted: 4

conditions), and August 5th for the rest of the GCAS flights as the instrument conditions were stable for the rest of the flight period. All reference spectra were co-located with total column NO_2 measurements from Pandora spectrometers: 5.6×10^{15} molecules cm^{-2} at MadisonCT on June 30th, 5.7×10^{15} molecules cm^{-2} at MadisonCT on July 2nd, and 6.2×10^{15} molecules cm^{-2} at WestportCT on August 5th, with values estimated to be over 50% stratospheric according to our TROPOMI bias corrected stratospheric column estimation (see below).

Fitted trace-gas absorption cross sections in the slant column spectral fit include NO_2 (Vandaele et al., 1998), O_4 (Thalman and Volkamer, 2013), water vapor (Rothman et al., 2009), CHOCHO (Volkamer et al., 2005), Ring spectrum (Chance and Kurucz, 2010), and a fifth-order polynomial. Average ± standard deviation spectral fitting uncertainties for the NO_2 slant columns during cloud-free scenes at cruising altitude for GeoTASO are $1.6\times10^{15} \pm 0.3\times10^{15}$ molecules cm^{-2} and for GCAS are $0.8\times10^{15} \pm 0.1\times10^{15}$ molecules cm^{-2}. The differences in uncertainty between spectral fits are likely due to a minor amount of under-sampling of the GeoTASO slit function, which has a slightly flattened top hat shape compared to the more purely Gaussian shape exhibited by GCAS.

Air mass factors (AMFs) are calculated using the Smithsonian Astrophysical Observatory AMF Tool (Nowlan et al., 2016 & 2018), which packages the VLIDORT radiative transfer model (Spurr, 2006) for calculating scattering weights based on user-inputs of viewing and solar geometries, a priori assumptions about surface reflectivity with Bidirectional Reflectance Distribution Function (BRDF) kernels, and meteorological and trace gas vertical profiles. AMFs are then calculated following the methodology of Palmer et al. (2001) as the integrated product of scattering weights and shape factor (e.g., Nowlan et al., 2016; Lamsal et al., 2017; Judd et al., 2019).

Table 1 compares a priori assumptions used for TROPOMI and airborne AMF calculations. For both retrievals, the spatial resolution of the a priori assumptions are coarser than those of the observations, but a priori assumptions for airborne observations are at a finer resolution than those for TROPOMI. Airborne a priori NO_2 vertical profile shapes are obtained for the troposphere from hourly output from a parallel developmental simulation of the North American Model–Community Multiscale Air Quality (NAMCMAQ) model from the National Air Quality Forecasting Capability (NAQFC; Stajner et al., 2011) and stratospheric NO_2 climatology developed using the PRATMO (PRather ATmospheric MOdel) (Prather, 1992; McLinden et al., 2000; Nowlan et al., 2016). The stratospheric column is bias corrected daily using TROPOMI NO_2 stratospheric vertical columns by calculating the average offset between the two datasets over the LISTOS domain for each day (ranging from $5x10^{13}$ to $6x10^{14}$ molecules cm^{-2}). This analysis only focuses on the below aircraft portion of the NO_2 columns from the aircraft, which is henceforth referred to as tropospheric vertical columns or TrVCs.

Surface reflectance over land is represented in the AMF tool input files with the isometric, geometric, and volumetric BRDF kernels given by the MODIS MCD43A1 product at 500m resolution at 470 nm averaged over the time period of the LISTOS campaign (Lucht et al., 2000; Schaaf and Wang, 2015). Input over water includes only the isometric BRDF kernel, limited to a minimum of 3% Lambertian reflectivity (similar to Nowlan et al., 2016), as well as an added Cox-Monk kernel (derived through references from Cox and Monk, 1954; Nakajima and Tanaka, 1983; Gordon and Wang, 1992; Spurr 2014;

Deleted: For slant to vertical column conversion,

Deleted: a

Deleted: Photochemical Box Model

and wind speed from the lowest layer of the NAM-CMAQ model and viewing and solar geometry). The brighter areas where the isometric BRDF kernel exceeds 3% are mostly over lakes, rivers, and coastlines rather than open water. Water surfaces are flagged using the Terra MODIS Land-Water Mask MOD44W product.

A temperature correction is applied within the air mass factor calculation (e.g., Bucsela et al., 2013) as the slant column retrievals only use an NO_2 absorption cross section at one temperature (294K). The temperature correction factor is the same factor used in the TROPOMI NO_2 product (van Geffen et al., 2019).

Clouds or aerosols are not accounted for in the AMF calculation in this analysis, though cloudy scenes are excluded from the analysis using a defined count rate threshold measured by the airborne spectrometer detector and visual verification from GOES 16 imagery (https://www.star.nesdis.noaa.gov/smcd/spb/aq/AerosolWatch/; last accessed 18 April 2020).

Differential slant columns are converted to below aircraft vertical columns (assumed as the tropospheric vertical column, TrVC) by subtracting the estimated stratospheric slant column (PRATMO climatology bias corrected daily with TROPOMI multiplied by the stratospheric AMF), adding the estimated reference slant column amount (from Pandora) and dividing by the tropospheric air mass factor, similar to Eq. 1 in Judd et al. (2019) or Eq 4. in Nowlan et al. (2018).

Previous work quantified uncertainty in airborne TrVCs from GCAS and GeoTASO by applying error propagation through the calculation of the vertical column based on uncertainties in the slant column fit, reference spectrum, and AMF calculation (Nowlan et al., 2016 & 2018; Judd et al., 2019). Relative uncertainties are largest for relatively clean sites (up to and over 100% in cases), however they decrease as pollution increases. Lorente et al. (2017) found that different methodologies applied to the same datasets can lead to structural uncertainty of 31-42%, which is mostly due to sensitivity to selection of a priori vertical profile shapes in the AMF calculation. In this work, airborne TrVCs are evaluated by comparing to Pandora NO_2 columns (Sect. 3) as Pandora NO_2 columns have relatively low uncertainties and their AMFs are not dependent on a priori profile shapes as described in the following section.

2.4 Pandora spectrometers

Deleted: 3

The Pandora instrument is a ground-based UV-VIS spectrometer that provides high-quality spectrally resolved direct sun/lunar or sky scan radiance measurements. The Pandora radiance measurements combine trace gas spectral fitting routines and, in the case of sky scan measurements, radiative transfer models to provide column densities of trace gas species similar to TROPOMI and airborne spectrometers. Pandora measurements obtained throughout the LISTOS study were limited to direct-sun mode, during which instrument tracks the sun to observe the direct-solar irradiance. Direct-sun columns are particularly beneficial for validation/evaluation due to their low uncertainties in the AMF (Herman et al., 2009). All data are processed as part of the Pandonia Global Network (PGN; www.pandonia-global-network.org) and only data with a quality flag of 0 or 10 (high quality) are used. Accuracy and precision of the total NO_2 column measurements from Pandora are reported as 2.69×10^{15} molecules cm^{-2}/AMF and $1.35x10^{14}$ molecules cm^{-2}, respectively (Herman et al. 2009; LuftBlick, 2016). All Pandora data are converted from total vertical columns to TrVCs by subtracting either the airborne estimated or TROPOMI retrieved stratospheric columns for comparison purposes.

Nine Pandora spectrometers were deployed and operated in the LISTOS domain in support of the LISTOS air quality study and as long-term measurements in support of EPA's Photochemical Assessment Monitoring Station Enhanced Monitoring (PAMS-EM) program (https://www3.epa.gov/ttnamti1/files/ambient/pams/PAMS%20EMP%20Guidance.pdf; last accessed 24 March 2020). Here, we use available Pandora data from these nine instruments between June 2018 and March 2019. There is one additional long-term Pandora located in NYC (CCNY campus, Instrument PI: M. Tzortziou) that is not part of the PAMS-EM program, and thus is not included in the quantitative analysis presented here. However, this instrument is used briefly to describe a case study in Sect 4.

The names, locations, and monthly days of operation of the 9 Pandora spectrometer sites used in this analysis are shown in Table 4. The grey shaded months indicate the time period of the LISTOS study. Figure 1 also shows the spatial distribution of these sites, which includes one site to the west of NYC (RutgersNJ), 3 instruments within the New York City metro area (BayonneNJ, BronxNY, and QueensNY), and 5 along the shoreline of Long Island Sound to the east-northeast of the city. Pandora sites were chosen to both capture upwind, in-city, and downwind emissions from NYC, particularly NO_2 transport down Long Island Sound from the city to help investigate the complex ozone pollution near this land/water interface. All instruments operated during the summer 2018 LISTOS campaign (defined as through September 2018), though four sites operated beyond LISTOS and are used in Sect. 5.2 for evaluation through 19 March 2019.

2.5 Methods

All linear regression statistics in this work are calculated using a Reduced Major Axis (RMA) including the coefficient of determination (r^2). This regression was chosen over Ordinary Least Squares (OLS) to recognize the potential for uncertainty in both evaluated and reference measurements. Percent and mean differences are also calculated and analysed and are calculated by the following convention:

$$\text{Column Difference} = \text{evaluated measurement} - \text{reference measurement}, \quad (1)$$

$$\text{Percent (\%) Difference} = \frac{\text{Column Difference}}{\text{reference measurement}} \times 100, \quad (2)$$

In Sects. 3 and 5, the reference measurements are the Pandora TrVCs and the evaluated measurements are the airborne and TROPOMI TrVCs, respectively. In Sect. 4, the reference measurements are the aircraft TrVCs and the evaluated measurements are TROPOMI NO_2 columns.

For all comparisons, coincidence criteria are chosen based on spatial, temporal, and physical components of the evaluated and reference measurements. In the following analysis, we use the following coincidence criteria (unless otherwise noted).

- For Pandora and airborne coincidences, the recommended coincidence criteria are from Judd et al. (2019), which are the median airborne TrVCs within a 750 m radius of the Pandora site and the temporally closest Pandora measurement (within ± 5 minutes of the aircraft overpass).
- For airborne comparisons to TROPOMI, each TROPOMI pixel must be at least 75% mapped by cloud-free airborne pixels within ± 30 minutes of the S5P overpass.

Deleted: Ten

Deleted: Here, we use available Pandora data from nine of the ten instruments between June 2018 and March 2019. Preliminary analysis indicated that data from one site (City College of New York (CCNY)) had a persistent though variable low bias relative to airborne data (not shown). This instrument is located on a building rooftop 113 m above ground level and is likely to be missing a portion of the TrVC associated with near surface NO_2 that would be observed by downward viewing instruments like TROPOMI and the airborne spectrometers. If co-located with coincident measurements nearer to the surface (e.g., Nowlan et al., 2016), this missing column could be estimated and applied, but due to the lack of such measurements this site was excluded from analysis.

Deleted: 4

Deleted: analyzed

- For Pandora comparisons to TROPOMI, the coincidence is identified by the TROPOMI pixel in which the Pandora is located (according to the TROPOMI pixel corners) and the median Pandora TrVC is calculated within ± 30 minutes of the S5P overpass.
- All TROPOMI data have cloud radiative fractions (CRFs) less than 50%. An additional new criterion is invoked to exclude points for which the difference between surface pressure and cloud pressure in the retrieval (as an indication of cloud height) exceeds 50 hPa. Justification of this criterion is discussed primarily in Sect. 4.1 and Sect. S3 and the influence of the criterion is considered throughout the paper.

Sensitivities to coincidence criteria are detailed in Tables S1-S3 and briefly discussed in each section and within the supplement to this manuscript.

In addition to the standard TROPOMI v1.2 NO_2 TrVC product we consider the effect of using a higher spatial resolution a priori NO_2 vertical profile shape in the TROPOMI retrieval. This is done by recalculating TROPOMI tropospheric AMF using the tropospheric averaging kernel to replace the TM5-MP a priori profile with the 12 km NAMCMAQ data used in the airborne spectrometer AMF calculations following the guidance provided in Sect 8.8 of Eskes et al. (2019).

3 Evaluating Airborne TrVC with Pandora Data

This work begins by comparing airborne and Pandora TrVC to evaluate the uncertainty of the airborne TrVCs and establish the spatial representativeness of the Pandora observations. This evaluation provides a consistent basis for using the high spatial resolution airborne data and high temporal resolution Pandora data to independently assess TROPOMI TrVCs.

During LISTOS, overflights of Pandora sites with the airborne spectrometers occurred during all 13 flight days spanning 25 June – 6 September 2018, between 12:00-22:00 UTC (08:00-18:00 EDT). Site-by-site scatter plots of all coincident measurements and linear regression statistics are shown in Fig. 2. At most sites the Pandora and airborne tropospheric NO_2 columns are highly correlated with slopes of approximately 1. Bars extending from each coincidence illustrate the spatial and temporal variability at the time of the measurements; the horizontal bars show the maximum and minimum Pandora observations within ± 5 minutes of the aircraft overpass and the vertical bars show the 10^{th}-90^{th} percentiles of the airborne pixels within a 750 m radius of the Pandora site (usually ~ 25-30 pixels). High temporal and spatial variations are mostly observed at polluted locations (e.g., QueensNY, BronxNY, and BayonneNJ). NewHavenCT has the lowest slope (0.71) of all sites yet a high correlation (r^2=0.87) which suggests a possible systematic site bias. Such a bias could be due to the inability of the MODIS BRDF product to resolve the spatial gradient of surface reflectance near this site, as this site is adjacent to both a bright urban area in New Haven and also the darker surface of the nearby river. Excluding MadisonCT, which has a poor linear regression due to the few (4) coincidences and small data range, the y-intercepts of the linear regressions range from -1.2 $\times 10^{15}$ to 2.0 $\times 10^{15}$ molecules cm^{-2}. The most likely cause for the range in y-intercepts between sites would be uncertainty in the estimated column for the reference spectrum in the Pandora retrieval, which uses the Minimum Langley Extrapolation (MLE) approach and has an estimated accuracy of 2.69×10^{15} molecules cm^{-2} for an AMF of 1 (Herman et al., 2009). The observed intercepts are all smaller than this estimated uncertainty.

Figure 3 shows the aggregated comparison of airborne and Pandora TrVC coincidences from all sites during LISTOS (n=171). Figure 3(a) shows the scatter plot and linear regression statistics. Each point is colored by the Pandora location, consistent with Fig. 2. Together, these data are highly correlated (r^2=0.92) with a slope of 1.03 and small offset of -0.4×10^{15} molecules cm^{-2}. Figure 3(a) also includes whiskers showing the spatial and temporal variability associated with each coincident observation similar to Fig. 2. Two different symbols are used as an objective indicator of temporal variability as quantified by Pandora observations; the outlined squares in Fig. 3(a) are coincidences where the Pandora TrVCs vary less than 30% within ± 15 minutes from the aircraft overpass (n=97) and the non-outlined circles indicate those exceeding 30% (n=74). (The temporal window for this assessment is larger than the ± 5 minutes shown in the max/min horizontal whiskers to include more data points to assess temporal variability.) Most of the temporally homogeneous points tightly span the 1:1 relationship, with the 95% falling within ± 25 % or have a difference less than 2.69x10^{15} molecules cm^{-2}. More of the temporally variable points expand further from the 1:1 line though still mostly fall within ± 50% or have a difference less than 2.69x10^{15} molecules cm^{-2} (98%). Considering only the temporally homogeneous measurements results in a very similar RMA fit (slope and offset) and a distinctly improved r^2 (0.96 vs. 0.92), but a loss of 43% of the number of data points (compare Table S1 Row H to Row B). This demonstrates the potential benefit of the high temporal resolution of Pandora observations for evaluating the impact of heterogeneity in NO_2 comparisons.

Previous work has suggested that the azimuth direction of the Pandora (due to its sunward viewing observations) can impact comparisons to airborne spectrometers in heterogeneously NO_2 polluted regions (Nowlan et al., 2018; Judd et al., 2019). We assessed this directionality sensitivity by also examining subsets of the airborne data within sectors surrounding Pandora's azimuth pointing direction (±22.5 and ±45-degree sectors were considered). The sector constraint slightly degrades the linear regression statistics, with an increase in slope 4-5%, decrease in y-intercept of 2-3x10^{14} molecules cm^{-2}, and no change in correlation (Table S1, compare Rows D and E to Row B). Considering directionality of Pandora can still be important in assessing individual cases but is not broadly implemented in this analysis due to the relative insensitivity found here and the limited feasibility of doing it in comparisons with the more spatially coarse measurements from satellites (including TROPOMI).

While most of the temporally homogeneous points are within ± 25% of each other, there are a small number of coincidences where the airborne spectrometer retrievals are more than 25% larger than Pandora. There were no clouds during these coincidences. The two Bronx coincidences that fall near the 1.25:1 line both occurred on 2 July 2018 during the morning and afternoon flights. The viewing direction of Pandora toward the southeast in the morning along with elevated NO_2 to the west of the site can partially explain the differences in the morning flight (as indicated by the large vertical whiskers for the green box near an airborne TrVC of 23×10^{15} molecules cm^{-2}), though in the afternoon, NO_2 is more homogeneous spatially near this location. Aerosols are elevated over the site on this day (HALO measured AOT at 532 nm is ~ 0.3), which could lead to a high bias in airborne TrVCs due to an underestimation in the AMF. However other coincidences during LISTOS also occurred with AOT of 0.3 or larger and there is no apparent correlation between AOT and the airborne/Pandora differences

(Fig. S1). Other coincidences on July 2nd (n=7) do not show a systematic aircraft high bias. The other temporally homogeneous high outlier occurred at Flax Pond on 29 August 2019 just after 13:00 UTC with no explanation related to the viewing direction of Pandora nor elevated aerosols (AOT ~ 0.16). This coincidence has the lowest calculated airborne tropospheric AMF (0.53), which may be too low due to the a priori profile being strongly weighted toward the surface than is in reality. The NAMCMAQ TrVC at this time is 1.7×10^{15} molecules cm^{-2} where 84% of that NO_2 is below 300m agl, suggesting too much near-surface NO_2 in this a priori profile. Less NO_2 near the surface in this a priori profile would increase the tropospheric AMF calculation at this site and a tropospheric AMF of 0.83 would bring this point into agreement with Pandora. The most likely reason for all these differences is incorrect vertical distribution and magnitude of NO_2 by the NAMCMAQ model and its influence on the tropospheric AMF (which would need to increase 27-64% to bring these cases into agreement with Pandora).

Figure 3(b) shows the difference between the airborne and Pandora observations as a function of time of day. Overall, there does not appear to be a dependence on time of day, which gives confidence that the airborne retrievals are correctly representing the effects of viewing and solar geometrical input, varying NO_2 a priori profiles through the day due to dynamic mixing and the growth of the boundary layer, and varying surface reflectivity based on the MODIS BRDF data in the radiative transfer model. Most (81%) of these differences are within $\pm 2.69\times10^{15}$ molecules cm^{-2}—the quoted accuracy of Pandora NO_2 retrievals in Herman et al. (2009). These results are encouraging for future validation studies of retrievals from data collected aboard geostationary platforms (e.g., TEMPO; Zoogman et al., 2017) with these types of airborne measurements. Considering only those coincidences during the overpass window of S5P (Table S1, compare Row B to Row I) slightly improves the correlation (r^2 increases from 0.92 to 0.94) but degrades the slope and intercept (slope increases from 1.03 to 1.13 with a compensating decrease in the y-intercept from -0.4 to -1.1×10^{15} molecules cm^{-2}). However, the median percent difference from Pandora is only 2% during this time period.

Figure 4 assesses the uncertainty of the airborne data and its potential sensitivity to pollution level. For the least polluted columns (below 3×10^{15} molecules cm^{-2}), the interquartile range of the column difference is within $\pm1\times10^{15}$ with a median of 0.1×10^{15}. For the more polluted columns, the interquartile range of the percent difference is mostly within 25% with a median difference within 0.6×10^{15} molecules cm^{-2}. These conclusions are not dependent on choice of 'reference' (i.e., the results are similar if examined as a function of binned airborne TrVC). For all data, the median percent difference is -1% with an interquartile range of -23 to 16%.

Considering all results between Pandora and the airborne spectrometers, uncertainty in the airborne spectrometer TrVC NO_2 is generally within ± 25% with no obvious bias overall. This uncertainty is lower than estimated using error propagation in previous literature, suggesting the errors in a priori datasets are smaller than was estimated in each study (Nowlan et al., 2016 & 2018; Judd et al., 2019).

Deleted: I

Deleted: B

Deleted: 3

4 Evaluating TROPOMI TrVC with Airborne Data

Airborne spectrometer data provide a spatially representative dataset in which to compare to TROPOMI with added information about subpixel variability. This is the first work that uses an airborne spectrometer dataset to evaluate the TROPOMI tropospheric NO_2 product.

During the LISTOS campaign, flight plans were designed with the intent to be airborne at the time of the S5P overpass. Figure 5 illustrates how the airborne data are matched to TROPOMI coincidences during three separate orbits—30 June, 19 July, and 6 September. The maps on the top row are true color imagery from the VIIRS sensor which overpasses approximately 5 minutes before S5P (data source: https://worldview.earthdata.nasa.gov/), showing that the first two days were clear of clouds but cumulus clouds were present during the 6 September overpass. The second row shows the overlaid TROPOMI TrVCs. NO_2 data are colored on a log10 scale spanning 1-100×10^{15} molecules cm^{-2}. These three cases illustrate how the day-to-day changes in spatial patterns and the dynamic range of NO_2 can be dramatically different from the annual average shown in Fig. 1 (note difference in color bar ranges between Fig. 5 and Fig. 1).

To compare the two datasets, coincident data following appropriate spatial, temporal, and other physical characteristics are extracted as discussed in Sect 2.5. The third row in Fig. 5 shows the airborne data that match the temporal coincidence criteria for these three orbits (± 30 min from the S5P overpass). The black outlines show TROPOMI pixels that are at least 75% mapped by the airborne spectrometers during this temporal window. Visually, the spatial patterns in TrVC observed by TROPOMI and the airborne instrument are consistent with each other. Finally, the subpixel airborne data within each TROPOMI pixel are gridded to a 250 m matrix to account for overlapping data from adjacent swaths and then the area weighted averages of the airborne TrVCs are computed to create values that are spatially and temporally consistent with the TROPOMI TrVC observations (bottom row in Fig. 5; gridding methodology from Kim et al., 2016).

From 25 June – 6 September 2018, the airborne spectrometers collected data that coincided with over 1300 TROPOMI pixels within ± 30 minutes of the S5P overpass. However, when considering only pixels 75% mapped by the airborne spectrometer and with CRF less than 50%, the number of coincidences decreases to 621. Additionally, through this analysis, we found that several notable outliers (coincidences with large apparent differences between the two measurements) corresponded with cloud retrieval effects in cloud-free scenes. Therefore, one additional coincidence criterion is applied to include only scenes with differences between the cloud pressure and surface pressures (Δ_{CS}) less than 50 hPa (the reported uncertainty of the cloud pressure retrieval in van Geffen et al., 2019). This criterion eliminates any TROPOMI pixels with assumed clouds and results in a reduction in the number of data points to 388. The impact of this criterion is discussed in Sect. 4.1 with an illustrative case study in Sect. S3 in the supplemental material, though points exceeding this coincidence criteria are still shown in scatter plots throughout this paper as blue crosses. (Statistics without this criterion are shown within Tables 5 and 7 and in the supplement).

Figure 6 shows scatterplot and linear regression statistics of all slant and vertical column coincidences between TROPOMI and the airborne data. The red circles in these plots represent the data that meet the strictest coincidence criteria

Deleted: to be used

Deleted: 4

discussed in the previous paragraph. For these points, the slant columns are very highly correlated (r^2=0.96). TROPOMI slant columns are consistently smaller than the airborne spectrometer slant columns (slope=0.59), though airborne slant columns are expected to be larger in comparison to satellite observations because the airborne spectrometers are more sensitive to altitudes nearer to the surface (where much of the NO_2 resides) due to the lower observational altitude of the aircraft. However, as shown by the high correlation, TROPOMI and the aircraft are sampling nearly the same atmosphere, at least in the lowest parts of the atmosphere that make up the majority of the TrVC. Converting from slant to vertical column increases (improves) the regression slope by 15% while preserving the very high correlation (r^2=0.96).

While the remaining low bias reflected by the slope below the 1:1 line will be discussed in subsequent sub-sections, we first begin with some discussion about potential reasoning for the small amount of scatter that exists between the TROPOMI and airborne measurements. These causes include: (1) a spatial component (i.e., we allow TROPOMI-scale airborne pixels to be missing data in up to 25% of the area of the TROPOMI pixel), (2) a temporal component as we allow up to 30 minutes difference between the time of the measurements, and (3) differing a priori assumptions made within each retrieval.

Considering the spatial component of scatter, the horizontal bars in Fig. 6 show the standard deviation of the subpixel airborne TrVCs within each TROPOMI pixel. Generally, the variation in subpixel NO_2 increases as the NO_2 TrVC increases, illustrating how scatter in the comparisons could increase if only small subsets of the pixel are mapped. Sensitivity to the mapped percentage is annotated in Table S2 (rows B-D and M-O) and shows little impact when relaxing the percent-mapped criterion to 50% (though is impacted negatively when the Δ_{CS} criterion is applied (Table S2: rows M-O)) and a more significant decrease when relaxing to 25%. At least with the airborne samples in this case, the linear statistics are driven by the most polluted pixels that are 100% mapped by the airborne spectrometers, explaining the limited sensitivity in the RMA fit to the percentage of the TROPOMI pixel mapped in this study.

Addressing the temporal component, if the temporal window is decreased to ± 15 minutes from ± 30 minutes, the number of mapped TROPOMI pixels by the aircraft decreases by 65% while the quality of linear statistics is moderately improved (Table S2, compare Row B to Row E). However, there is a larger adverse impact to the RMA fit and r^2 when the time window is extended to extract airborne data within ± 60 minutes of the S5P overpass. Coincidences occurring between 30-60 minutes from the S5P overpass are shown as open circles in Fig. 6. For example, the small subset of very polluted airborne TrVCs that are much larger than what is retrieved by TROPOMI occurred during a time with high temporal variability on 2 July 2018. The airborne spectrometer observed a distinct very polluted plume over NYC and over the 48-minute period between the airborne and TROPOMI observations, the Pandora spectrometer located at the CCNY observed a 50% decrease in NO_2 total vertical column, leading to a large difference between the airborne and TROPOMI TrVCs when the temporal window is extended to ± 60 min (M. Tzortziou, personal communication).

These outliers are caused by real spatiotemporal variability rather than issues in either of the retrievals and demonstrate the care needed for matching airborne data collected over time to the nearly instantaneous observations from S5P TROPOMI. These large differences are also apparent in the slant column comparisons and future studies should consider slant column comparison between aircraft and TROPOMI as a guide for identifying potential spatial and temporal mismatches.

Deleted:), even for cases with large sub-pixel variation as indicated by the horizontal whiskers in the plot

Deleted: of

Deleted: a Pandora spectrometer located at the CCNY observed a 50% decrease in NO_2 total vertical column, leading to a large difference between the airborne and TROPOMI TrVCs when the temporal window is extended to ± 60 min. (Note that because the CCNY Pandora is placed well above the surface it was excluded from the airborne and TROPOMI comparisons and no other Pandora instruments coincided with this feature).

With respect to differing retrieval assumptions, we consider two factors in the following subsections: treatment of clouds and NO_2 vertical profile shape.

4.1 Cloud retrieval effects

In previous literature, a coincidence criterion based on CRF from TROPOMI has been the common consideration for data comparisons, though studies vary slightly in their chosen CRF threshold (ranging from 30-50% in Griffin et al. (2019), Ialongo et al. (2020), and Zhao et al. (2020)). We investigate the effect on the statistics of varying CRF threshold, alone, but find that retrieved cloud height is also an important factor and here consider the two effects together.

In the TROPOMI retrieval, surface reflectivity is estimated using the 0.5° × 0.5° climatology from five years of OMI observations (Kleipool et al., 2008; van Geffen et al., 2019). When the surface albedo climatology used for TROPOMI has a low bias, which can occur over bright city centers, the algorithm increases the overall brightness of the scene by assuming a non-zero cloud fraction. In cloud-free urban scenes, this approach generally results in a non-zero CRF with a nominal cloud pressure equal to the surface pressure. Fig. S2(a) illustrates this behavior on a cloud-free day (19 July 2018).

This CRF-adjustment approach over bright surfaces generally appears to work well, however we identified a potential issue when the retrieval also places retrieved "clouds" above the surface rather than at the surface in cloud-free scenes. The two most obvious illustrations of this effect are evident as the two blue crosses farthest above the regression line with airborne TrVCs greater than 25×10^{15} molecules cm^{-2} in Fig. 6. Section S3 in the supplemental material presents a case study demonstrating that the effect is correctable for these two points. We note that in the presence of significant scattering aerosols, CRF may also be larger than zero and the cloud pressure level may mimic the height of the aerosol layer. During aircraft coincidences with TROPOMI, the average AOT at 532 nm measured by HALO was 0.22 with a standard deviation of 0.15. In the case of these outliers, elevated aerosol loading has been ruled out (AOT at 532 nm was 0.04). Clouds and their effect on the estimated vertical sensitivity are an important component within the NO_2 retrieval, as clouds are assumed to 'shield' the view of the atmosphere below the cloud level in some fractions of the pixel. However, in cloud-free scenes, cloud pressures significantly less than the surface pressure with elevated CRF can lead to an underestimation in the AMF, and therefore an overestimation in TROPOMI TrVC, as the shielding that is assumed through the retrieval is not occurring in reality. Because the airborne screening criteria ensure that only cloud-free observations are included in our analysis, our comparisons are biased toward cloud-free scenes, and therefore high CRFs are associated generally with bright surfaces instead of clouds.

To avoid these impacts, we explored an additional coincidence criterion based on cloud parameters in the TROPOMI product file. We consider an allowable difference between retrieved cloud pressure and surface pressure (henceforth Δ_{CS}) of less than 50 hPa (which is the reported uncertainty in cloud pressure retrieval from van Geffen et al., 2019). Figure 6 shows points that exceed this criterion as blue cross symbols and the linear regression statistics with and without this criterion applied are summarized in Table 5. Applying this criterion removes approximately 30% of coincidences including the largest outliers but also many points that are not outliers. Of the 233 data points that have Δ_{CS} greater than 50 hPa, 58% (n=136) of them have

Deleted: ,

Deleted: however

Deleted: i

Deleted: is

Deleted: by the HALO measurements co-located with the airborne spectrometer

aircraft measured cloud fractions of less than 2%, and 69% of these cloud free coincidences (n=94) have reported CRFs greater than 10%, illustrating that the cloud retrieval regularly yields an effective cloud height above the surface even during cloud-free scenes. Further filtering data by only removing data with CRFs > 10% results in very little change in the overall statistics. Table 5 shows that the largest impact of the Δ_{CS} criterion is an improvement in the correlation (r^2 of 0.96 vs. 0.90) but a slope further from 1 (0.68 vs. 0.71) and a more negative median percent difference (-19% vs -11%), showing that there is excellent correlation between the two measurements but an apparent low bias in the TROPOMI retrieval that the cloud pressure errors partially offset. This impact is also confined to the TrVC comparisons and not apparent in the slant column comparisons, which demonstrates the impact is through assumptions made in the AMF calculation.

Eskes and Eichmann (2019) mention occurrences of negative effective cloud fractions in the FRESCO cloud product that could also result in positive cloud fraction in the NO_2 window in v1.2 of the TROPOMI TrVC product which causes a noisy NO_2 retrieval. The occurrence of negative FRESCO cloud fractions with positive CRFs did occur during many of these coincidences (63% of the 621 pixels). However, this fraction is much lower for Δ_{CS} flagged pixels (18%) and they were not associated with the largest outliers in this analysis. Applying a criterion to remove negative cloud fractions instead of Δ_{CS} flagged pixels results in similar results as only filtering for CRFs < 50% and no Δ_{CS} criterion (slope=0.72, offset=0.7×10^{15} molecules cm^{-2}, r^2=0.91, and n=233). Therefore, this impact is not the cause for the described patterns in the previous paragraph.

In the vertical columns, coincidences identified by the Δ_{CS} criterion typically lie above the best-fit line, consistent with the hypothesis of effective cloud shielding in the AMF calculation during cloud-free scenes. There is one obvious coincidence exceeding the Δ_{CS} threshold that opposes this general pattern by falling below the best fit line (blue cross with airborne TrVC around 50×10^{15} molecules cm^{-2}). This apparent disparity appears to be caused by large temporal variation between the times of the airborne and satellite measurements. The airborne measurement preceded TROPOMI by 23 minutes and in a subsequent airborne measurement over the same area 70 minutes later, the airborne NO_2 TrVC had decreased to approximately 30×10^{15} molecules cm^{-2}, which is much nearer to the TROPOMI-measured value of 25×10^{15} molecules cm^{-2}. This is another example where a temporal mismatch resulted in an outlier in the slant column comparisons in Fig. 6(a) demonstrating the use of slant column comparisons to assist in identifying spatial and temporal mismatches.

Finally, we summarize the sensitivity to different CRF thresholds. Without the Δ_{CS} criterion applied (Table S2; Rows F-I), allowing larger CRF values generally decreases r^2 while increasing the slope slightly and dramatically increasing the number of coincidences. Highest correlations, up to 0.96, are maintained with CRF < 20%. When the Δ_{CS} threshold is applied, the RMA fit is largely insensitive to changes in CRF up to 50% (Table S2: Rows J-M), maintaining the high quality of the linear regression while including progressively more data points with increasing CRF thresholds. Because CRF can often exceed 20% over urban areas even in cloud free conditions due to effects of the coarse a priori surface reflectivity used in the retrieval, the Δ_{CS} criterion appears useful for retaining valid cloud-free coincidences over bright urban scenes. Overall, the best fit is attained either by restricting CRF to less than 20% and not using the Δ_{CS} criterion or by using the Δ_{CS} criterion, which allows

inclusion of CRF values up to 50% and provides 35% more coincidences. Future research could explore using alternative cloud measurements (e.g., from VIIRS) to identify cloud-free scenes and the use of clear-sky AMFs.

4.2 NO_2 vertical profile shape

The a priori vertical profiles in the TROPOMI NO_2 retrieval are from the TM5-MP model with a spatial resolution of 1° × 1° interpolated to the center of the TROPOMI pixels (van Geffen et al., 2019). In a heterogeneously polluted region such as NYC, NO_2 profiles vary at much smaller spatial scales. For spatial reference, the area flown by the airborne spectrometer flights for each LISTOS raster (Fig. 1) cover an area of approximately 1° × 1° or smaller and airborne TrVCs span up to two orders of magnitude in this domain. Here, TROPOMI tropospheric AMFs are recalculated with the 12 km NAMCMAQ analysis used in the airborne TrVC retrieval to demonstrate the impact of spatial resolution of a priori profiles. These TROPOMI TrVCs columns are hereafter labeled as TROPOMI-NAMCMAQ. The original TROPOMI v1.2 product is referred to as TROPOMI Standard.

Figure 7 has the same format as Fig. 6 but instead compares TROPOMI-NAMCMAQ to airborne TrVCs. (Note that both datasets are now using the same a priori profiles.) In general, applying the NAMCMAQ profile into the TROPOMI AMF calculation brings the airborne and TROPOMI data into closer agreement; with the Δ_{CS} criterion applied, slope increases 13% from 0.68 to 0.77, the median percent difference improves from -19% to -7%, and a high r^2 is maintained (changing from 0.96 to 0.95).

Incorporating a higher resolution a priori profile appears to result in an increase in the sensitivity to the Δ_{CS} criterion, with more of the blue cross points visible in Fig. 7 than in Fig. 6, which can likely be attributed to increased sensitivity to the lower altitude levels in the AMF calculation. In the higher resolution NAMCMAQ analysis, the lower levels are more polluted and thus more sensitive to 'cloud' shielding.

The biases of the TROPOMI Standard and TROPOMI-NAMCMAQ TrVCs with respect to the airborne data are further examined as a function of pollution level in Fig. 8. The majority of points (68%) are less than 6×10^{15} molecules cm^{-2}, so the overall distributions are dominated by the behavior in the lowest bins in Fig. 8. In these lowest two bins, the median percent difference is -10% and +3%, respectively for TROPOMI Standard and TROPOMI-NAMCMAQ TrVCs. Column differences unsurprisingly increase with pollution level and are small in these two lowest bins, with the interquartile range within 1×10^{15} molecules cm^{-2} and inner 90% of points having differences within 2×10^{15} molecules cm^{-2}. TROPOMI Standard has a median absolute bias of zero in the lowest bin. Using the NAMCMAQ profile shifts the bias more positive in all bins, creating a small positive bias in the lowest bin but reducing the overall median bias from -1×10^{15} molecules cm^{-2} to 0.3×10^{15} molecules cm^{-2}. For airborne TrVCs above 6×10^{15} molecules cm^{-2}, the median percent difference is -29% for the TROPOMI Standard but improves to -20% for TROPOMI-NAMCMAQ. Although a higher resolution a priori profile improves the overall bias in the TROPOMI product, there is still a low bias for the most polluted TROPOMI TrVCs columns.

5 Evaluating TROPOMI TrVC with Pandora Data

Pandoras operated in the LISTOS domain during and after the conclusion of the intensive LISTOS airborne measurements as part of the PAMS EM Program (see Table 4). Following coincidence criteria in line with those from Sect. 4 (TROPOMI CRF < 50%, Δ_{CS} less than 50hPa, and median Pandora TrVC within ±30 minutes), Fig. 9 shows all coincidences between Pandora and TROPOMI through 19 March 2019, with coincidences during the LISTOS intensive period (defined as any measurements prior to and including 30 September 2018) outlined in black. Site-by-site statistics are listed in Table 6 for both time periods. In this section we discuss consistency in TROPOMI evaluation results with airborne spectrometers using data from only the LISTOS time period and also from an extended temporal window at select sites that operated through winter 2019.

5.1 TROPOMI v. Pandora during LISTOS

During the LISTOS time period, there were 156 coincidences between the nine Pandora spectrometers and TROPOMI, ranging from 8 to 25 coincidences by site (Table 6). With the exception of MadisonCT and BranfordCT (which lack in TrVC dynamic range), the slope of TROPOMI vs. Pandora is less than one (ranging from 0.49-0.84, similar to the results in Sect. 4) with moderate to high values of r^2 (0.29-0.90). All median percent differences are negative and vary by site ranging from -9% to -52%.

Figure 10(a) shows the aggregated TROPOMI Standard and Pandora dataset during LISTOS; red circles/blue crosses are those that have a Δ_{CS} less than/greater than 50hPa, respectively, similar to Fig. 6. The bars represent the reported precision of the TROPOMI Standard product (vertical) and the 10^{th}-90^{th} percentile of Pandora data within the ± 30 min window (horizontal). Temporal variation of TrVCs measured by Pandora increases proportionally to pollution level (r^2=0.69). The aggregated dataset shows that TROPOMI TrVCs have a low bias in comparison to Pandora (slope=0.80 and offset of -0.7×10^{15} molecules cm^{-2}) and high correlation (r^2=0.84). As a whole, TROPOMI has a median percent difference from Pandora of -33% with an interquartile range of -48% to -14%, consistent with comparisons of TROPOMI to airborne TrVCs for values above 6×10^{15} molecules cm^{-2}. Comparing Fig. 10(a) to Fig. 6(b), the slope is 18% higher (better) than in the comparisons to the TROPOMI Standard product to airborne TrVCs, though at the expense of a lower r^2 (0.96 vs. 0.84). Coincidences at QueensNY and BronxNY have the lowest median percent difference of all the sites and the aggregate slope is sensitive to whether these two sites are included or not (0.80 and 0.72 with and without BronxNY and QueensNY, respectively). This result highlights the sensitivity of site selection and duration in the combined analysis and can likely be attributed to differences in spatial representivity between the TROPOMI and Pandora and perhaps sampling temporally over just the short period of the LISTOS study.

Spatial representivity of Pandora and sub-pixel variation in the TROPOMI area can also influence the results. TROPOMI pixels span an areal coverage of approximately 30-130 km^2 depending on the position in the swath through S5P's 16-day orbit cycle, while Pandora measurements represent a more localized environment. We found that the interquartile range

of the TROPOMI bias relative to Pandora becomes slightly more negative as the pixel size gets larger (not shown). For pixels less than 40km^2, the interquartile range is -1% to -46% (n=67), whereas for pixels larger than 80km^2, it is -14% to -59% (n=18).

Unlike with airborne spectrometer data comparisons, sub-TROPOMI pixel cloud information is not readily available for these comparisons to Pandora. However, the impact of coincidence criteria based on clouds is assessed similarly to Sect. 4. Lowering of the CRF threshold preferentially excludes data from sites with brighter surface reflectivity and, typically, larger NO_2 values. For example, QueensNY has a median CRF of 34% (minimum of 17%), whereas a more rural location like WestportCT has a median CRF of 8% (minimum of 0%). Without applying the Δ_{CS} criterion, we find the quality of the linear regression statistics to be quite sensitive to CRF threshold (Table S3, Rows F-I). Using more restrictive CRF thresholds generally worsens the correlation and the trends here are less consistent than found in the TROPOMI-airborne comparisons. This inconsistency is due to the relatively fewer number of Pandora coincidences having large values, e.g. above 10×10^{15} molecules cm^{-2}, which makes the linear regression sensitive to screening criteria such as CRF that exclude any of the larger-valued data points. Though applying the Δ_{CS} criterion removes nearly half the coincidences for CRFs < 50%, its application increases r^2 values at all CRF thresholds (Table S3; Rows J-M). Applying the Δ_{CS} criterion maintains high correlations while allowing retention of data from bright urban sites that would be preferentially left out by filtering by CRF for thresholds 30% and lower.

Figure 10(b) shows the comparison between TROPOMI-NAMCMAQ TrVCs and Pandora. Many more coincidences with Δ_{CS} greater than 50hPa (blue crosses) are evident above the 1:1 line, again illustrating the increased sensitivity to this parameter when higher resolution a priori profiles are used within the TROPOMI AMF calculation. Table 7 summarizes all the various cases. Considering all coincidences without invoking the Δ_{CS} criterion (i.e., including blue crosses and red circles), there is a large improvement in the regression statistics from TROPOMI Standard to TROPOMI-NAMCMAQ, with the slope closer to 1 and a median percent difference of only -9% (relative to the -30% for TROPOMI Standard). However, as illustrated by the blue points in Fig. 10(b), it is clear that this 'improvement' is partially driven by a high bias related to the impact of clouds. When points with Δ_{CS} greater than 50hPa are excluded, the slope between TROPOMI-NAMCMAQ and Pandora improves by only 2.5% in comparison to TROPOMI Standard with a slight degradation of r^2 from 0.84 to 0.80. However, there is a large improvement in the median percent difference, from -33% (interquartile range of -48% to -14%) for TROPOMI Standard to -19% (interquartile range of -36 to 5%) for TROPOMI-NAMCMAQ.

Much of the correlation in Fig. 10 is driven by the 20 points above 10×10^{15} molecules cm^{-2}; considering only points below 10×10^{15} molecules cm^{-2} lowers r^2 to 0.42 and 0.39 for TROPOMI Standard and TROPOMI-NAMCMAQ, respectively, though results in the same median percent differences. The loss in correlation demonstrates the challenge of doing linear regressions on datasets with a lack of dynamic range well above 10×10^{15} molecules cm^{-2} in this analysis when spatiotemporal variability impacts can be at a similar magnitude. However, extending analysis through winter 2019 results in a larger sampled dynamic range as demonstrated in the next section.

Deleted: Although

Deleted: for

Deleted: Pandora

Deleted: at TROPOMI sub-pixel resolution is not readily available

Deleted: ,

5.2 TROPOMI v. Pandora through 19 March 2019

The deployment of many of the Pandora instruments in this region as part of the PAMS EM Program presents the opportunity for evaluation beyond the period of the LISTOS intensive campaign. TROPOMI level 2 NO_2 processing switched to version 1.3 after 19 March 2019, thus this analysis goes only through this date to avoid possible influences associated with the version change. To ensure consistent spatial representivity through the period, analysis is limited to the four sites that continued operation through 19 March 2019 (Table 4; RutgersNJ, BayonneNJ, QueensNY, and WestportCT). The focus of this extended analysis is to see whether conclusions made from the LISTOS time period are still valid through the fall and winter months as photochemistry and meteorological changes lead to potential shifts in spatial and temporal variation and dynamic range at these sites. These four sites represent two in-city sites and sites upwind and downwind from NYC, though the upwind/downwind side of the city is dependent on wind direction from day-to-day. Figure 11 shows timeseries of Pandora and TROPOMI Standard TrVCs from 25 June 2018 through 19 March 2019 at each of the sites. Colored circles represent the Pandora measurements during the S5P overpass, the black stars show the TROPOMI TrVC, and the whiskers indicate variability or uncertainty (see figure caption). Note that some days have two overpasses. In general, temporal patterns are similar in both TROPOMI and Pandora measurements demonstrating each instruments ability to observe synoptic and seasonal variability in TrVCs.

At RutgersNJ and WestportCT, Pandora and TROPOMI TrVCs rarely exceed 10×10^{15} molecules cm^{-2} during the year. More polluted coincidences occurred periodically during November-March as expected given the longer photochemical lifetime of NO_2 during winter. In early January, when both Pandora and TROPOMI values were low, the spatial distribution of NO_2 in the LISTOS domain from TROPOMI showed that the NYC plume was advected over the Atlantic Ocean on most of these days and was not intercepted by either site. At WestportCT, there was an extended period of elevated columns near the end of January and beginning of February. The larger TrVC values during that period coincide with days when the NYC plume extends toward Long Island Sound and Connecticut, likely driven by synoptic flow from the southwest quadrant. (This is the flow orientation that is often linked with poor ozone air quality along the shorelines of Long Island Sound during the summertime, e.g., the late August 2018 timeframe which was active with respect to ozone (airnow.gov: last accessed 11 March 2019) but did not result in an NO_2 enhancement over WestportCT, likely due to the shorter NO_2 lifetime in summer.) Alternatively, at RutgersNJ on the 9th of March, the Pandora site was encompassed by an NO_2 plume extending from the center of NYC during two consecutive TROPOMI overpasses leading to its maximum TrVC values during the time period assessed. Unlike the other two sites, BayonneNJ and QueensNY have large dynamic ranges in NO_2 TrVCs in all seasons due to their proximity to strong sources within the NYC metropolitan area. Extending comparisons through the winter allows for more frequently measuring large values to extend the dynamic range of the coincident measurements.

Figure 11(e) shows the percent difference in TROPOMI TrVCs from Pandora with the bars showing the temporal variability of these percent differences during the ± 30-minute temporal window from the S5P overpass (10th-90th percentile). Despite some changes seasonally in the magnitude of NO_2 at each of the sites, the percent difference in TROPOMI from

Pandora does not have an apparent significant trend over this time period. The majority of points fall within 0% to -50%. The points with percent differences closest to zero, including points with positive percent differences, are associated with small values at WestportCT. Many of the coincidences have very large ranges in percent difference due to the temporal variability of Pandora TrVCs within the ± 30-minute time period that are likely associated with sub-pixel heterogeneity, again illustrating the challenge of quantifying biases with Pandora in urban environments.

Figure 12 shows a scatter plot of the coincidences at these four sites during both the LISTOS timeframe (Fig. 12(a)) and the longer 9-month period (Fig. 12(b)). During the LISTOS period the slope is 0.76 and a reasonably high r^2 of 0.89 is caused by the large range of TrVCs observed at BayonneNJ and QueensNY. These results are similar to those at all nine locations during the LISTOS timeframe (Fig. 10(a)) with the same median percent difference. The number of coincidences through the LISTOS months is low (n=58) due to the Δ_{CS} threshold being frequently exceeded (Table 7). The number and dynamic range of observations is greater when extended through the rest of the year (n=195). The overall median percent difference is 8% lower over the 9-month period (-27%) than the LISTOS timeframe (-19%), and though it is not visually apparent in Fig. 11(e), this drop is reflected by a decrease in the median percent difference at QueensNY (Table 6). At QueensNY, the median percent difference for TrVCs becomes more negative at higher magnitudes of TrVC; Pandora TrVCs less than/greater than 15×10^{15} molecules cm^{-2} have a median percent difference of -15% and -33%, respectively, at this site. Despite large day-to-day variations and changes in dynamic range through the seasons, the linear statistics for the aggregated data at these four sites are largely unchanged when comparing the LISTOS time frame to the extended 9-month period (2.5% difference in slope and 0.01 range in r^2).

6 Overall evaluation of TROPOMI v1.2 NO_2 TrVCs

Tables 5 and 7 summarize the overall results of TROPOMI TrVC comparisons to the airborne and Pandora spectrometers from this work. No matter the reference dataset or data selection criteria, linear regression and percent difference statistics indicate that in this urban coastal region the v1.2 TROPOMI Standard TrVC product has a low bias. Median TROPOMI NO_2 TrVCs are 19% and 33% lower than airborne and Pandora TrVCs, respectively, during the LISTOS timeframe. These different values are partially related to the characteristics of sampling at different TrVC ranges between the two datasets. One-third (130) of the airborne coincidences have TrVC less than 3×10^{15} molecules cm^{-2} with no observed bias between the two measurements, while only 19 of the 156 Pandora coincidences have TrVC less than 3×10^{15} molecules cm^{-2} with TROPOMI having a low bias of -21% at these cleanest levels. At higher TrVC magnitudes (greater than 6×10^{15} molecules cm^{-2}), the percent differences of TROPOMI from aircraft (-29%) and Pandora (-31%) are more similar to each other. Lesser polluted columns are more sensitive to uncertainties related to the stratospheric columns, references, and other assumptions (which are different between all retrievals), whereas at more polluted levels the bias is more attributed to uncertainties in tropospheric air mass factors.

Overall these results are consistent with other studies using independent measurements to evaluate the TROPOMI NO_2 products, as they also found that the TROPOMI NO_2 product has a low bias in the Canadian Oil Sands (Griffin et al.,

Deleted: Pandora spectrometers

2019), Toronto, Canada (Zhao et al., 2019), Paris, France (Lorente et al., 2019), polluted scenes (> 10×10^{15} molecules cm^{-2}) near Helsinki (Ialongo et al., 2020), Brussels, Belgium (Dimitropoulou et al., 2020), China (Liu et al., 2020), and Munich, Germany (Chan et al., 2020). Verhoelst et al. (2020) completed a comprehensive analysis of TROPOMI NO_2 products using broad networks of Pandora direct-sun and MAX-DOAS observations and also saw a low bias in the tropospheric product, including consistent results with three Pandoras used in this analysis (QueensNY, BronxNY, and BayonneNJ) with similar patterns in results (e.g., BronxNY, QueensNY, and BayonneNJ having a median percent difference of -15%, -23%, -41% (this work) vs. -13%, -26%, -31% (Verhoelst et al., 2020), respectively). Slight differences are expected due to different date windows and coincidence criteria. Many of these studies found improvement by using higher resolution regional model a priori profile shapes in the AMF calculation for TROPOMI. In this study, recalculating the TROPOMI tropospheric AMF with the higher resolution 12 km NAMCMAQ analysis resolves some of the low bias in TROPOMI TrVCs, improving median percent differences from -19% to -7% with respect to airborne data and from -33% to -19% with respect to Pandora data. However, despite this improvement, there is still a persistent low bias in the TROPOMI TrVCs.

This analysis is impacted by influences of cloud pressure in the TROPOMI retrieval. Invoking the Δ_{CS} criterion increases (worsens) the overall TROPOMI low bias as it removes a high bias caused by assumed cloud shielding in the AMF calculation in cloud-free scenes. In all comparisons shown in Tables 5 and 7, the median percent difference is more negative (worse) when only points with Δ_{CS} less than 50 hPa are included, and the effect is more pronounced for TROPOMI-NAMCMAQ coincidences (decreasing 10-11%) than for TROPOMI Standard (decreasing 4-8%). Invoking the criterion also consistently improves the correlation in every case by removing many of the outlier points, as intended. The most striking examples are the airborne comparison with TROPOMI-NAMCMAQ (r^2 improved from 0.83 to 0.95) and Pandora comparison with TROPOMI-Standard for the 4-site subset of the LISTOS period (r^2 improved from 0.79 to 0.88).

7 Conclusions

The operational nature of the S5P TROPOMI mission as part of the Copernicus Program marks an important step forward in monitoring of the environment, amplifying the need for increased validation capacity of satellite trace gas data. The datasets collected in support of the Long Island Sound Tropospheric Ozone Study during summer 2018 and as part of the PAMS-EM program are exceptional for evaluation of TROPOMI TrVCs, providing a robust set of independent remotely sensed NO_2 column densities from airborne spectrometers (13 mapping flights from 25 June 2018 to 6 September 2018) and a network of nine ground-based Pandora spectrometer systems.

Previous studies have shown that Pandora direct-sun NO_2 columns are valuable for validating airborne spectrometer retrievals due to their high precision and temporal resolution and comparable spatial resolution (e.g., Nowlan et al., 2016; Judd et al., 2019). In this study, the airborne spectrometer data are highly correlated with Pandora measurements with a slope of 1.03, offset of -0.4×10^{15} molecules cm^{-2}, and r^2=0.92. Much of the remaining scatter in the data can be attributed to the spatiotemporal heterogeneity of NO_2 in this urban coastal environment, as evaluating only the less temporally varying

Deleted: and

measurements shows similar statistics but a higher r^2 of 0.96. Though singular comparisons can exceed differences of 25%, overall the majority of the coincidences fall well within ±25% and 81% of the coincidences fall within the reported accuracy of Pandora of 2.69×10^{15} molecules cm^{-2}. These results give confidence for using both datasets to assess the TROPOMI TrVC product.

The combination of these two reference measurements in one region presents unique strengths for validation of TROPOMI TrVCs over a domain with large variations in NO_2. Pandora measurements are useful for evaluating space-based and aircraft-based retrievals due to their ability to observe continuously in one location for long time periods. However, the impact of subpixel heterogeneity within satellite pixel areas can lead to mismatches between the Pandora and satellite despite the much-improved spatial resolution of TROPOMI. Airborne spectrometers are typically only deployed for short periods of time, but their observations are more spatially representative of the satellite measurements with the added capability of retrieving at subpixel resolutions over the entire TROPOMI pixel areas they overfly. In this study, the strengths of the two reference measurements were able to be combined. TROPOMI comparisons to airborne TrVCs are more correlated than Pandora comparisons during the LISTOS timeframe (r^2=0.96 vs. 0.84). Additionally, the long-term deployment of Pandora instruments as part of the PAMS-EM program allowed TROPOMI TrVCs to be assessed over multiple seasons. We find the strongest impact of seasonality is the extension of the TrVC dynamic range sampled in the winter months, providing more robust statistical fits though not very significant changes in the statistics overall between the two time periods.

During the LISTOS timeframe, TROPOMI Standard TrVC data have a low bias in comparison to Pandora and airborne TrVCs of -33% and -19%, respectively. This bias improves to -19% and -7% when TROPOMI TrVCs are recalculated using AMFs with the 12 km NAMCMAQ a priori profile. These results are obtained by screening out cases where cloud shielding estimated in the TROPOMI retrieval occurred over cloud free scenes, which tend to compensate partially for the TROPOMI TrVC low bias and introduce significant artifacts that degrade correlations with reference measurements. Future exploration of cloud-based coincidence criteria would help in identifying effects of cloud parameters on NO_2 trace gas comparisons and other evaluations of near-surface weighted trace gases such as HCHO. It will also help in evaluating how these sensitivities change as cloud retrievals and their implementation into the trace-gas retrievals evolve in future versions (e.g., in v1.3, implemented after 19 March 2019, the FRESCO-S cloud retrieval was updated adjust surface albedo in cloud-free areas where the surface albedo climatology is too low, as discussed in Eskes and Eichmann, 2019).

We find the v1.2 TROPOMI Standard TrVCs to be within the validation requirements for the mission (bias within ± 25-50%; van Geffen et al., 2019) but with a persistent low bias in the NYC region. While some of the bias is removed by the incorporation of a higher resolution a priori vertical profile, there is still a low bias in the TROPOMI NO_2 TrVC retrieval which indicates the need for improved a priori assumptions in the AMF calculations. This analysis looked at the impacts of a priori NO_2 profiles at a moderately higher resolution and of clouds, and future work should also explore effects of surface reflectivity. A component not explicitly explored in this work, that could be in the future, is the potential impact of aerosols on the TROPOMI retrieval and whether their indirect accounting through the cloud retrieval accurately reflects the impacts within the radiative transfer calculations for the air mass factor calculation (e.g., Leitão et al., 2010; Ma et al., 2013; Jin et al.,

Deleted: sub-

Deleted: is

Deleted: an

Deleted: amd

Deleted: low

2016). Some differences between TROPOMI and airborne TrVCs can be related to differences in a priori assumptions between the TROPOMI and airborne retrievals; Lorente et al. (2017) discussed that the structural uncertainty in tropospheric air mass factors is up to 42% in polluted regions due to different retrieval methodologies. Future comparisons should consider using common methodologies for AMF calculation for both airborne and TROPOMI TrVCs to better quantify the sensitivity of specific a priori assumptions in AMF calculations.

This work is the first dataset that has used airborne spectrometer measurements to evaluate a satellite NO_2 retrieval at this degree of success (large number of coincidences, high correlation, and mapping 100% of pixel areas) which is supportive of using airborne spectrometers to validate and evaluate UV-VIS trace gas retrievals during current and future satellite missions, including geostationary measurements. This LISTOS dataset, as well as future ones collected during other intensive field studies, will be useful for continuing to evaluate the TROPOMI algorithms through future releases of the TROPOMI NO_2 TrVC product.

Author Contribution

LMJ prepared the manuscript with contributions from all co-authors. JAA, LCV, JJS, RBP, and LMJ led flight planning activities for LISTOS. SJJ, MGK, and LMJ collected the airborne spectrometer data and AN collected HALO data during LISTOS flights. LMJ processed the airborne spectrometer NO_2 retrievals. RBP provided the NAM-CMAQ analysis used in the vertical column retrieval and in reprocessing of TROPOMI data. CRN and GGA provided the Smithsonian Astrophysical Observatory AMF Tool as well as guidance in its use for AMF calculations. HJE and JPV provided their expertise in the TROPOMI product and discussed results periodically through this project. JJS, DW, LCV, and RS led the coordination, installation, and maintenance of Pandora spectrometers in the LISTOS domain. AC, MM, and MG led the processing of the Pandora NO_2 retrievals and provided guidance in Pandora data analysis.

Deleted: coauthors

Acknowledgements

Authors would like to acknowledge Peter Pantina and Sanxiong Xiong for their participation in airborne data collection during LISTOS flights, members of the HALO team for supporting flights and data processing of aerosol optical depth, Nader Abuhassan and Lena Shalaby for their assistance in installing and monitoring the Pandora network in the LISTOS domain, extending to the larger Pandora teams at NASA GSFC and LuftBlick through their support in Pandora data processing. The LISTOS airborne measurements would not have been possible without the support of the NASA GEO-CAPE Mission Study as well as NASA ESD Tropospheric Composition Program. We express gratitude to the entire LISTOS science team for their expertise, research, and measurement contributions toward the successful collaborative field study. Finally, we would like to give recognition and thanks to Maria Tzortziou for contributing information about the Pandora located at CCNY.

This work is done in part through the Sentinel-5P Validation Team Projects 28695 and 40030. This work contains modified Copernicus data.

Disclaimer: The research described in this article has been reviewed by the U.S. Environmental Protection Agency (EPA) and approved for publication. Approval does not signify that the contents necessarily reflect the views and the policies of the agency nor does mention of trade names or commercial products constitute endorsement or recommendation for use.

Data Availability

TROPOMI: https://s5phub.copernicus.eu/dhus/#/home

Airborne spectrometer data version R0: https://www-air.larc.nasa.gov/cgi-bin/ArcView/listos

Pandora data can be found at www.pandonia-global-network.org. QueensNY, BayonneNJ, and BronxNY have been processed with versions rnvs1p1-7 and the rest of the sites were processed with rnvs0p1-5. On the official PGN webpage just the nvs1p1-7 data will be accessible as soon as the data is available. There is no difference between the products except the data flagging procedures.

References

Anenberg, S. C., Henze, D. K., Tinney, V., Kinney, P. L., Raich, W., Fann, N., Malley, C. S., Roman, H., Lamsal, L., Duncan, B., Martin, R. V., van Donkelaar, A., Brauer, M., Doherty, R., Jonson, J. E., Davila, Y., Sudo, K. and Kuylenstierna, J. C. I.: Estimates of the Global Burden of Ambient PM2.5, Ozone, and NO2 on Asthma Incidence and Emergency Room Visits, Environmental Health Perspectives, 126(10), 107004, doi:10.1289/EHP3766, 2018.

Behrens, L. K., Hilboll, A., Richter, A., Peters, E., Eskes, H. and Burrows, J. P.: GOME-2A retrievals of tropospheric NO2 in different spectral ranges – influence of penetration depth, Atmospheric Measurement Techniques, 11(5), 2769–2795, doi:10.5194/amt-11-2769-2018, 2018.

Beirle, S., Boersma, K. F., Platt, U., Lawrence, M. G. and Wagner, T.: Megacity Emissions and Lifetimes of Nitrogen Oxides Probed from Space, Science, 333(6050), 1737–1739, doi:10.1126/science.1207824, 2011.

Beirle, S., Borger, C., Dörner, S., Li, A., Hu, Z., Liu, F., Wang, Y. and Wagner, T.: Pinpointing nitrogen oxide emissions from space, Science Advances, 5(11), eaax9800, doi:10.1126/sciadv.aax9800, 2019.

Boersma, K. F., Eskes, H. J., Dirksen, R. J., van der A, R. J., Veefkind, J. P., Stammes, P., Huijnen, V., Kleipool, Q. L., Sneep, M., Claas, J., Leitão, J., Richter, A., Zhou, Y. and Brunner, D.: An improved tropospheric NO2 column retrieval algorithm for

the Ozone Monitoring Instrument, Atmospheric Measurement Techniques, 4(9), 1905–1928, doi:10.5194/amt-4-1905-2011, 2011.

Boersma, K. F., Eskes, H. J., Richter, A., De Smedt, I., Lorente, A., Beirle, S., van Geffen, J. H. G. M., Zara, M., Peters, E., Van Roozendael, M., Wagner, T., Maasakkers, J. D., van der A, R. J., Nightingale, J., De Rudder, A., Irie, H., Pinardi, G., Lambert, J.-C. and Compernolle, S. C.: Improving algorithms and uncertainty estimates for satellite NO2 retrievals: results from the quality assurance for the essential climate variables (QA4ECV) project, Atmospheric Measurement Techniques, 11(12), 6651–6678, doi:10.5194/amt-11-6651-2018, 2018.

Borsdorff, T., Aan de Brugh, J., Hu, H., Aben, I., Hasekamp, O. and Landgraf, J.: Measuring Carbon Monoxide With TROPOMI: First Results and a Comparison With ECMWF-IFS Analysis Data, Geophysical Research Letters, 45(6), 2826–2832, doi:10.1002/2018GL077045, 2018.

Bovensmann, H., Burrows, J. P., Buchwitz, M., Frerick, J., Noël, S., Rozanov, V. V., Chance, K. V. and Goede, A. P. H.: SCIAMACHY: Mission objectives and measurement modes, Journal of the atmospheric sciences, 56(2), 127–150, 1999.

Broccardo, S., Heue, K.-P., Walter, D., Meyer, C., Kokhanovsky, A., van der A, R., Piketh, S., Langerman, K. and Platt, U.: Intra-pixel variability in satellite tropospheric NO2 column densities derived from simultaneous space-borne and airborne observations over the South African Highveld, Atmospheric Measurement Techniques, 11(5), 2797–2819, doi:10.5194/amt-11-2797-2018, 2018.

Bucsela, E. J., Krotkov, N. A., Celarier, E. A., Lamsal, L. N., Swartz, W. H., Bhartia, P. K., Boersma, K. F., Veefkind, J. P., Gleason, J. F. and Pickering, K. E.: A new stratospheric and tropospheric NO2 retrieval algorithm for nadir-viewing satellite instruments: applications to OMI, Atmos. Meas. Tech., 6(10), 2607–2626, doi:10.5194/amt-6-2607-2013, 2013.

Burrows, J. P., Weber, M., Buchwitz, M., Rozanov, V., Ladstätter-Weißenmayer, A., Richter, A., DeBeek, R., Hoogen, R., Bramstedt, K. and Eichmann, K.-U.: The global ozone monitoring experiment (GOME): Mission concept and first scientific results, Journal of the Atmospheric Sciences, 56(2), 151–175, 1999.

Callies, J., Corpaccioli, E., Eisinger, M., Hahne, A. and Lefebvre, A.: GOME-2-Metop's second-generation sensor for operational ozone monitoring, ESA bulletin, 102, 28–36, 2000.

Chan, K. L., Wiegner, M., Alberti, C., and Wenig, M.: MAX-DOAS measurements of tropospheric NO_2 and HCHO in Munich and the comparison to OMI and TROPOMI satellite observations, Atmos. Meas. Tech. Discuss., https://doi.org/10.5194/amt-2020-35, in review, 2020.

Chance, K. and Kurucz, R. L.: An improved high-resolution solar reference spectrum for earth's atmosphere measurements in the ultraviolet, visible, and near infrared, Journal of Quantitative Spectroscopy and Radiative Transfer, 111(9), 1289–1295, doi:10.1016/j.jqsrt.2010.01.036, 2010.

Cox, C. and Munk, W.: Measurement of the Roughness of the Sea Surface from Photographs of the Sun's Glitter, J. Opt. Soc. Am., JOSA, 44(11), 838–850, doi:10.1364/JOSA.44.000838, 1954.

De Smedt, I., Theys, N., Yu, H., Danckaert, T., Lerot, C., Compernolle, S., Van Roozendael, M., Richter, A., Hilboll, A., Peters, E., Pedergnana, M., Loyola, D., Beirle, S., Wagner, T., Eskes, H., van Geffen, J., Boersma, K. F. and Veefkind, P.: Algorithm Theoretical Baseline for formaldehyde retrievals from S5P TROPOMI and from the QA4ECV project, Atmospheric Measurement Techniques Discussions, 1–53, doi:10.5194/amt-2017-393, 2017.

Dimitropoulou, E., Hendrick, F., Pinardi, G., Friedrich, M. M., Merlaud, A., Tack, F., De Longueville, H., Fayt, C., Hermans, C., Laffineur, Q., Fierens, F., and Van Roozendael, M.: Validation of TROPOMI tropospheric NO_2 columns using dual-scan MAX-DOAS measurements in Uccle, Brussels, Atmos. Meas. Tech. Discuss., https://doi.org/10.5194/amt-2020-33, in review, 2020.

Eskes, H. and Eichmann, K.-U.: S5P Mission Performance Centre Nitrogen Dioxide [L2__NO2___] Readme. http://www.tropomi.eu/sites/default/files/files/publicSentinel-5P-Nitrogen-Dioxide-Level-2-Product-Readme-File_20191105.pdf (Accessed 14 April 2020), 2019.

Eskes, H., van Geffen, J., Boersma, F., Eichmann, K.-U., Apituley, A., Pedergnana, M., Sneep, M., Veefkind, J. P. and Loyola, D.: Sentinel-5 precursor/TROPOMI Level 2 Product User Manual Nitrogen dioxide, http://www.tropomi.eu/sites/default/files/files/publicS5P-KNMI-L2-0021-MA-Product_User_Manual_for_the_Sentinel_5_precursor_Nitrogen_dioxide-3.0.0-20190327.pdf (Accessed 14 April 2020), 2019.

Fischer, P. H., Marra, M., Ameling, C. B., Hoek, G., Beelen, R., de Hoogh, K., Breugelmans, O., Kruize, H., Janssen, N. A. H. and Houthuijs, D.: Air Pollution and Mortality in Seven Million Adults: The Dutch Environmental Longitudinal Study (DUELS), Environ. Health Perspect., 123(7), 697–704, doi:10.1289/ehp.1408254, 2015.

Garane, K., Koukouli, M.-E., Verhoelst, T., Lerot, C., Heue, K.-P., Fioletov, V., Balis, D., Bais, A., Bazureau, A., Dehn, A., Goutail, F., Granville, J., Griffin, D., Hubert, D., Keppens, A., Lambert, J.-C., Loyola, D., McLinden, C., Pazmino, A., Pommereau, J.-P., Redondas, A., Romahn, F., Valks, P., Van Roozendael, M., Xu, J., Zehner, C., Zerefos, C. and Zimmer, W.: TROPOMI/S5P total ozone column data: global ground-based validation and consistency with other satellite missions, Atmospheric Measurement Techniques, 12(10), 5263–5287, doi:10.5194/amt-12-5263-2019, 2019.

van Geffen, J., Eskes, H., Boersma, F., Maasakkers, J. D. and Veefkind, J. P.: TROPOMI ATBD of the total and tropospheric NO2 data products. http://www.tropomi.eu/sites/default/files/files/publicS5P-KNMI-L2-0005-RP-ATBD_NO2_data_products-20190206_v140.pdf (Accessed 14 April 2020), 2019.

van Geffen, J., Boersma, K. F., Eskes, H., Sneep, M., ter Linden, M., Zara, M. and Veefkind, J. P.: S5P TROPOMI NO2 slant column retrieval: method, stability, uncertainties and comparisons with OMI, Atmospheric Measurement Techniques, 13(3), 1315–1335, doi:10.5194/amt-13-1315-2020, 2020.

Goldberg, D. L., Lamsal, L. N., Loughner, C. P., Swartz, W. H., Lu, Z. and Streets, D. G.: A high-resolution and observationally constrained OMI NO2 satellite retrieval, Atmospheric Chemistry and Physics, 17(18), 11403–11421, doi:10.5194/acp-17-11403-2017, 2017.

Goldberg, D. L., Lu, Z., Streets, D. G., de Foy, B., Griffin, D., McLinden, C. A., Lamsal, L. N., Krotkov, N. A. and Eskes, H.: Enhanced Capabilities of TROPOMI NO2 : Estimating NOx from North American Cities and Power Plants, Environmental Science & Technology, 53(21), 12594–12601, doi:10.1021/acs.est.9b04488, 2019.

González Abad, G., Souri, A. H., Bak, J., Chance, K., Flynn, L. E., Krotkov, N. A., Lamsal, L., Li, C., Liu, X., Miller, C. C., Nowlan, C. R., Suleiman, R. and Wang, H.: Five decades observing Earth's atmospheric trace gases using ultraviolet and visible backscatter solar radiation from space, Journal of Quantitative Spectroscopy and Radiative Transfer, 238, 106478, doi:10.1016/j.jqsrt.2019.04.030, 2019.

Gordon, H. R. and Wang, M.: Surface-roughness considerations for atmospheric correction of ocean color sensors 1: The Rayleigh-scattering component, Applied Optics, 31(21), 4247, doi:10.1364/AO.31.004247, 1992.

Griffin, D., Zhao, X., McLinden, C. A., Boersma, F., Bourassa, A., Dammers, E., Degenstein, D., Eskes, H., Fehr, L., Fioletov, V., Hayden, K., Kharol, S. K., Li, S.-M., Makar, P., Martin, R. V., Mihele, C., Mittermeier, R. L., Krotkov, N., Sneep, M., Lamsal, L. N., Linden, M. ter, Geffen, J. van, Veefkind, P. and Wolde, M.: High-Resolution Mapping of Nitrogen Dioxide

With TROPOMI: First Results and Validation Over the Canadian Oil Sands, Geophysical Research Letters, 46(2), 1049–1060, doi:10.1029/2018GL081095, 2019.

Herman, J., Cede, A., Spinei, E., Mount, G., Tzortziou, M. and Abuhassan, N.: NO2 column amounts from ground-based Pandora and MFDOAS spectrometers using the direct-sun DOAS technique: Intercomparisons and application to OMI validation, Journal of Geophysical Research, 114(D13), doi:10.1029/2009JD011848, 2009.

Hu, H., Landgraf, J., Detmers, R., Borsdorff, T., Brugh, J. A. de, Aben, I., Butz, A. and Hasekamp, O.: Toward Global Mapping of Methane With TROPOMI: First Results and Intersatellite Comparison to GOSAT, Geophysical Research Letters, 45(8), 3682–3689, doi:10.1002/2018GL077259, 2018.

Ialongo, I., Virta, H., Eskes, H., Hovila, J. and Douros, J.: Comparison of TROPOMI/Sentinel-5 Precursor NO2 observations with ground-based measurements in Helsinki, Atmospheric Measurement Techniques, 13(1), 205–218, doi:10.5194/amt-13-205-2020, 2020.

Janz, S., Judd L., and Kowalewski, M.: Long Island Sound Tropospheric Ozone Study GeoTASO/GCAS NO2 Vertical Columns, NASA ASDC Lake Michigan Ozone Study Repository, available at: https://www-air.larc.nasa.gov/missions/listos/index.html, last access: 14 April 2020.

Jin, J., Ma, J., Lin, W., Zhao, H., Shaiganfar, R., Beirle, S., Wagner, T. MAX-DOAS measurements and satellite validation of tropospheric NO2 and SO2 vertical column densities at a rural site of North China. Atmos. Environ. 133, 12–25. https://doi.org/10.1016/j.atmosenv.2016.03.031, 2016

Judd, L. M., Al-Saadi, J. A., Valin, L. C., Pierce, R. B., Yang, K., Janz, S. J., Kowalewski, M. G., Szykman, J. J., Tiefengraber, M. and Mueller, M.: The Dawn of Geostationary Air Quality Monitoring: Case Studies From Seoul and Los Angeles, Front. Environ. Sci., 6, doi:10.3389/fenvs.2018.00085, 2018.

Judd, L. M., Al-Saadi, J. A., Janz, S. J., Kowalewski, M. G., Pierce, R. B., Szykman, J. J., Valin, L. C., Swap, R., Cede, A., Mueller, M., Tiefengraber, M., Abuhassan, N. and Williams, D.: Evaluating the impact of spatial resolution on tropospheric NO2 column comparisons within urban areas using high-resolution airborne data, Atmospheric Measurement Techniques, 12(11), 6091–6111, doi:https://doi.org/10.5194/amt-12-6091-2019, 2019.

Kim, H. C., Lee, P., Judd, L., Pan, L. and Lefer, B.: OMI NO2 column densities over North American urban cities: the effect of satellite footprint resolution, Geoscientific Model Development, 9(3), 1111–1123, doi:10.5194/gmd-9-1111-2016, 2016.

Kleipool, Q. L., Dobber, M. R., Haan, J. F. de and Levelt, P. F.: Earth surface reflectance climatology from 3 years of OMI data, Journal of Geophysical Research: Atmospheres, 113(D18), doi:10.1029/2008JD010290, 2008.

Kowalewski, M. G. and Janz, S. J.: Remote sensing capabilities of the GEO-CAPE airborne simulator, SPIE Conference Proceedings, San Diego, California, United States., 2014. https://doi.org/10.1117/12.2062058

Lamsal, L. N., Krotkov, N. A., Celarier, E. A., Swartz, W. H., Pickering, K. E., Bucsela, E. J., Gleason, J. F., Martin, R. V., Philip, S., Irie, H., Cede, A., Herman, J., Weinheimer, A., Szykman, J. J. and Knepp, T. N.: Evaluation of OMI operational standard NO_2 column retrievals using in situ and surface-based NO_2 observations, Atmospheric Chemistry and Physics, 14(21), 11587–11609, doi:10.5194/acp-14-11587-2014, 2014.

Lamsal, L. N., Janz, S. J., Krotkov, N. A., Pickering, K. E., Spurr, R. J. D., Kowalewski, M. G., Loughner, C. P., Crawford, J. H., Swartz, W. H. and Herman, J. R.: High-resolution NO2 observations from the Airborne Compact Atmospheric Mapper: Retrieval and validation: High-Resolution NO $_2$ Observations, Journal of Geophysical Research: Atmospheres, 122(3), 1953–1970, doi:10.1002/2016JD025483, 2017.

Lawrence, J. P., Anand, J. S., Vande Hey, J. D., White, J., Leigh, R. R., Monks, P. S. and Leigh, R. J.: High-resolution measurements from the airborne Atmospheric Nitrogen Dioxide Imager (ANDI), Atmospheric Measurement Techniques, 8(11), 4735–4754, doi:10.5194/amt-8-4735-2015, 2015.

Leitão, J., Richter, A., Vrekoussis, M., Kokhanovsky, A., Zhang, Q. J., Beekmann, M. and Burrows, J. P.: On the improvement of NO2 satellite retrievals – aerosol impact on the airmass factors, Atmos. Meas. Tech., 19, 2010.

Leitch, J. W., Delker, T., Good, W., Ruppert, L., Murcray, F., Chance, K., Liu, X., Nowlan, C., Janz, S. J., Krotkov, N. A., Pickering, K. E., Kowalewski, M. and Wang, J.: The GeoTASO airborne spectrometer project, edited by J. J. Butler, X. (Jack) Xiong, and X. Gu, p. 92181H., 2014.

Levelt, P. F., Oord, G. H. J. van den, Dobber, M. R., Malkki, A., Visser, H., Vries, J. de, Stammes, P., Lundell, J. O. V. and Saari, H.: The ozone monitoring instrument, IEEE Transactions on Geoscience and Remote Sensing, 44(5), 1093–1101, doi:10.1109/TGRS.2006.872333, 2006.

Levelt, P. F., Joiner, J., Tamminen, J., Veefkind, J. P., Bhartia, P. K., Stein Zweers, D. C., Duncan, B. N., Streets, D. G., Eskes, H., van der A, R., McLinden, C., Fioletov, V., Carn, S., de Laat, J., DeLand, M., Marchenko, S., McPeters, R., Ziemke, J., Fu,

D., Liu, X., Pickering, K., Apituley, A., González Abad, G., Arola, A., Boersma, F., Chan Miller, C., Chance, K., de Graaf, M., Hakkarainen, J., Hassinen, S., Ialongo, I., Kleipool, Q., Krotkov, N., Li, C., Lamsal, L., Newman, P., Nowlan, C., Suleiman, R., Tilstra, L. G., Torres, O., Wang, H. and Wargan, K.: The Ozone Monitoring Instrument: overview of 14 years in space, Atmospheric Chemistry and Physics, 18(8), 5699–5745, doi:10.5194/acp-18-5699-2018, 2018.

Liang, J., Horowitz, L. W., Jacob, D. J., Wang, Y., Fiore, A. M., Logan, J. A., Gardner, G. M. and Munger, J. W.: Seasonal budgets of reactive nitrogen species and ozone over the United States, and export fluxes to the global atmosphere, J. Geophys. Res., 103(D11), 13435–13450, doi:10.1029/97JD03126, 1998.

Liu, F., Beirle, S., Zhang, Q., Dörner, S., He, K. and Wagner, T.: NOx lifetimes and emissions of cities and power plants in polluted background estimated by satellite observations, Atmospheric Chemistry and Physics, 16(8), 5283–5298, doi:10.5194/acp-16-5283-2016, 2016.

Liu, M., Lin, J., Kong, H., Boersma, K. F., Eskes, H., Kanaya, Y., He, Q., Tian, X., Qin, K., Xie, P., Spurr, R., Ni, R., Yan, Y., Weng, H., and Wang, J.: A new TROPOMI product for tropospheric NO_2 columns over East Asia with explicit aerosol corrections, Atmos. Meas. Tech., 13, 4247–4259, https://doi.org/10.5194/amt-13-4247-2020, 2020.

Lorente, A., Folkert Boersma, K., Yu, H., Dörner, S., Hilboll, A., Richter, A., Liu, M., Lamsal, L. N., Barkley, M., De Smedt, I., Van Roozendael, M., Wang, Y., Wagner, T., Beirle, S., Lin, J.-T., Krotkov, N., Stammes, P., Wang, P., Eskes, H. J. and Krol, M.: Structural uncertainty in air mass factor calculation for NO2 and HCHO satellite retrievals, Atmospheric Measurement Techniques, 10(3), 759–782, doi:10.5194/amt-10-759-2017, 2017.

Lorente, A., Boersma, K. F., Eskes, H. J., Veefkind, J. P., van Geffen, J. H. G. M., de Zeeuw, M. B., Denier van der Gon, H. A. C., Beirle, S. and Krol, M. C.: Quantification of nitrogen oxides emissions from build-up of pollution over Paris with TROPOMI, Scientific Reports, 9(1), doi:10.1038/s41598-019-56428-5, 2019.

Loyola, D.: S5P/TROPOMI Clouds ATBD. http://www.tropomi.eu/sites/default/files/files/Sentinel-5P-TROPOMI-ATBD-Clouds_20180430_signed.pdf (Accessed 14 April 2020), 2018.

Lucht, W., Schaaf, C. B. and Strahler, A. H.: An algorithm for the retrieval of albedo from space using semiempirical BRDF models, IEEE Transactions on Geoscience and Remote Sensing, 38(2), 977–998, doi:10.1109/36.841980, 2000.

Ludewig, A., Kleipool, Q., Bartstra, R., Landzaat, R., Leloux, J., Loots, E., Meijering, P., van der Plas, E., Rozemeijer, N., Vonk, F. and Veefkind, P.: In-flight calibration results of the TROPOMI payload on-board theSentinel-5 Precursor satellite, preprint, Gases/Remote Sensing/Instruments and Platforms., 2020.

LuftBlick: ESA Ground-Based Air-Quality Spectrometer Validation Network and Uncertainties Study, [online] Available from: https://www.pandonia-global-network.org/wp-content/uploads/2019/06/LuftBlick_Pandonia_TraceGasRetrievalFeasibilityStudy_RP_2016001_v1.1.pdf (Accessed 14 April 2020), 2016.

Ma, J. Z., Beirle, S., Jin, J. L., Shaiganfar, R., Yan, P. and Wagner, T.: Tropospheric NO_2 vertical column densities over Beijing: results of the first three years of ground-based MAX-DOAS measurements (2008-2011) and satellite validation, Atmospheric Chemistry and Physics, 13(3), 1547–1567, doi:10.5194/acp-13-1547-2013, 2013.

McLinden, C. A., Olsen, S. C., Hannegan, B., Wild, O., Prather, M. J. and Sundet, J.: Stratospheric ozone in 3-D models: A simple chemistry and the cross-tropopause flux, Journal of Geophysical Research: Atmospheres, 105(D11), 14653–14665, doi:10.1029/2000JD900124, 2000.

Meier, A. C., Schönhardt, A., Bösch, T., Richter, A., Seyler, A., Ruhtz, T., Constantin, D.-E., Shaiganfar, R., Wagner, T., Merlaud, A., Roozendael, M. V., Belegante, L., Nicolae, D., Georgescu, L. and Burrows, J. P.: High-resolution airborne imaging DOAS measurements of NO2 above Bucharest during AROMAT, Atmos. Meas. Tech., 27, 2017.

Nakajima, T. and Tanaka, M.: Effect of wind-generated waves on the transfer of solar radiation in the atmosphere-ocean system, Journal of Quantitative Spectroscopy and Radiative Transfer, 29(6), 521–537, doi:10.1016/0022-4073(83)90129-2, 1983.

Nehrir, A., Notari, A., Harper, D., Fitzpatrick, F., Collins, J., Kooi, S., Antill, C., Hare, R., Barton-Grimley, R., Hair, J., Ferrare, R., Hostetler, C. and Welch, W.: The High Altitude Lidar Observatory (HALO): A multi-function lidar and technology test-bed for airborne and space-based measurements of water vapor and methane, [online] Available from: https://esto.nasa.gov/forum/ESTF2018/presentations/Nehrir_ESTF2018_A1P2.pdf (Accessed 14 April 2020), 2018.

Nowlan, C. R., Liu, X., Leitch, J. W., Chance, K., González Abad, G., Liu, C., Zoogman, P., Cole, J., Delker, T., Good, W., Murcray, F., Ruppert, L., Soo, D., Follette-Cook, M. B., Janz, S. J., Kowalewski, M. G., Loughner, C. P., Pickering, K. E., Herman, J. R., Beaver, M. R., Long, R. W., Szykman, J. J., Judd, L. M., Kelley, P., Luke, W. T., Ren, X. and Al-Saadi, J. A.: Nitrogen dioxide observations from the Geostationary Trace gas and Aerosol Sensor Optimization (GeoTASO) airborne

instrument: Retrieval algorithm and measurements during DISCOVER-AQ Texas 2013, Atmospheric Measurement Techniques, 9(6), 2647–2668, doi:10.5194/amt-9-2647-2016, 2016.

Nowlan, C. R., Liu, X., Janz, S. J., Kowalewski, M. G., Chance, K., Follette-Cook, M. B., Fried, A., González Abad, G., Herman, J. R., Judd, L. M., Kwon, H.-A., Loughner, C. P., Pickering, K. E., Richter, D., Spinei, E., Walega, J., Weibring, P. and Weinheimer, A. J.: Nitrogen dioxide and formaldehyde measurements from the GEOstationary Coastal and Air Pollution Events (GEO-CAPE) Airborne Simulator over Houston, Texas, Atmospheric Measurement Techniques Discussions, 1–36, doi:10.5194/amt-2018-156, 2018.

Palmer, P. I., Jacob, D. J., Chance, K., Martin, R. V., Spurr, R. J. D., Kurosu, T. P., Bey, I., Yantosca, R., Fiore, A. and Li, Q.: Air mass factor formulation for spectroscopic measurements from satellites: Application to formaldehyde retrievals from the Global Ozone Monitoring Experiment, J. Geophys. Res., 106(D13), 14539–14550, doi:10.1029/2000JD900772, 2001.

Pierce, R. B., Schaack, T., Al-Saadi, J. A., Fairlie, T. D., Kittaka, C., Lingenfelser, G., Natarajan, M., Olson, J., Soja, A., Zapotocny, T., Lenzen, A., Stobie, J., Johnson, D., Avery, M. A., Sachse, G. W., Thompson, A., Cohen, R., Dibb, J. E., Crawford, J., Rault, D., Martin, R., Szykman, J., and Fishman, J.: Impacts of background ozone production on Houston and Dallas, Texas, air quality during the Second Texas Air Quality Study field mission, J. Geophys. Res., 114, D00F09, https://doi.org/10.1029/2008JD011337, 2009.

Platt, U. and Stutz, J.: Differential optical absorption spectroscopy: principles and applications ; with 55 tables, Springer, Berlin., 2008.

Popp, C., Brunner, D., Damm, A., Van Roozendael, M., Fayt, C. and Buchmann, B.: High-resolution NO2 remote sensing from the Airborne Prism EXperiment (APEX) imaging spectrometer, Atmospheric Measurement Techniques, 5(9), 2211–2225, doi:10.5194/amt-5-2211-2012, 2012.

Prather, M.: Catastrophic loss of stratospheric ozone in dense volcanic clouds, Journal of Geophysical Research: Atmospheres, 97(D9), 10187–10191, doi:10.1029/92JD00845, 1992.

Reed, A. J., Thompson, A. M., Kollonige, D. E., Martins, D. K., Tzortziou, M. A., Herman, J. R., Berkoff, T. A., Abuhassan, N. K. and Cede, A.: Effects of local meteorology and aerosols on ozone and nitrogen dioxide retrievals from OMI and pandora spectrometers in Maryland, USA during DISCOVER-AQ 2011, J Atmos Chem, 72(3–4), 455–482, doi:10.1007/s10874-013-9254-9, 2015.

Rothman, L. S., Gordon, I. E., Barbe, A., Benner, D. C., Bernath, P. F., Birk, M., Boudon, V., Brown, L. R., Campargue, A., Champion, J.-P., Chance, K., Coudert, L. H., Dana, V., Devi, V. M., Fally, S., Flaud, J.-M., Gamache, R. R., Goldman, A., Jacquemart, D., Kleiner, I., Lacome, N., Lafferty, W. J., Mandin, J.-Y., Massie, S. T., Mikhailenko, S. N., Miller, C. E., Moazzen-Ahmadi, N., Naumenko, O. V., Nikitin, A. V., Orphal, J., Perevalov, V. I., Perrin, A., Predoi-Cross, A., Rinsland, C. P., Rotger, M., Šimečková, M., Smith, M. A. H., Sung, K., Tashkun, S. A., Tennyson, J., Toth, R. A., Vandaele, A. C. and Vander Auwera, J.: The HITRAN 2008 molecular spectroscopic database, Journal of Quantitative Spectroscopy and Radiative Transfer, 110(9–10), 533–572, doi:10.1016/j.jqsrt.2009.02.013, 2009.

Schaaf, C. and Wang, Z.: MCD43A1 MODIS/Terra+Aqua BRDF/Albedo Model Parameters Daily L3 Global - 500m V006, , doi:10.5067/MODIS/MCD43A1.006, 2015.

Schönhardt, A., Altube, P., Gerilowski, K., Krautwurst, S., Hartmann, J., Meier, A. C., Richter, A. and Burrows, J. P.: A wide field-of-view imaging DOAS instrument for two-dimensional trace gas mapping from aircraft, Atmospheric Measurement Techniques, 8(12), 5113–5131, doi:10.5194/amt-8-5113-2015, 2015.

Souri, A. H., Choi, Y., Pan, S., Curci, G., Nowlan, C. R., Janz, S. J., Kowalewski, M. G., Liu, J., Herman, J. R. and Weinheimer, A. J.: First Top-Down Estimates of Anthropogenic NOx Emissions Using High-Resolution Airborne Remote Sensing Observations, Journal of Geophysical Research: Atmospheres, 123(6), 3269–3284, doi:10.1002/2017JD028009, 2018.

Souri, A. H., Nowlan, C. R., Wolfe, G. M., Lamsal, L. N., Chan Miller, C. E., Abad, G. G., Janz, S. J., Fried, A., Blake, D. R., Weinheimer, A. J., Diskin, G. S., Liu, X. and Chance, K.: Revisiting the effectiveness of HCHO/NO2 ratios for inferring ozone sensitivity to its precursors using high resolution airborne remote sensing observations in a high ozone episode during the KORUS-AQ campaign, Atmospheric Environment, 224, 117341, doi:10.1016/j.atmosenv.2020.117341, 2020.

Spurr, R.: VLIDORT Version 2.7 User's Guide, 2014.

Spurr, R. J. D.: VLIDORT: A linearized pseudo-spherical vector discrete ordinate radiative transfer code for forward model and retrieval studies in multilayer multiple scattering media, Journal of Quantitative Spectroscopy and Radiative Transfer, 102(2), 316–342, doi:10.1016/j.jqsrt.2006.05.005, 2006.

Stajner, I., Davidson, P., Byun, D., McQueen, J., Draxler, R., Dickerson, P. and Meagher, J.: US National Air Quality Forecast Capability: Expanding Coverage to Include Particulate Matter, in Air Pollution Modeling and its Application XXI, edited by D. G. Steyn and S. Trini Castelli, pp. 379–384, Springer Netherlands., 2012.

Tack, F., Merlaud, A., Iordache, M.-D., Danckaert, T., Yu, H., Fayt, C., Meuleman, K., Deutsch, F., Fierens, F. and Van Roozendael, M.: High-resolution mapping of the NO2 spatial distribution over Belgian urban areas based on airborne APEX remote sensing, Atmospheric Measurement Techniques, 10(5), 1665, 2017.

Tack, F., Merlaud, A., Meier, A. C., Vlemmix, T., Ruhtz, T., Iordache, M.-D., Ge, X., van der Wal, L., Schuettemeyer, D., Ardelean, M., Calcan, A., Constantin, D., Schönhardt, A., Meuleman, K., Richter, A. and Van Roozendael, M.: Intercomparison of four airborne imaging DOAS systems for tropospheric NO2 mapping – the AROMAPEX campaign, Atmospheric Measurement Techniques, 12(1), 211–236, doi:10.5194/amt-12-211-2019, 2019.

Thalman, R. and Volkamer, R.: Temperature dependent absorption cross-sections of O2–O2 collision pairs between 340 and 630 nm and at atmospherically relevant pressure, Physical Chemistry Chemical Physics, 15(37), 15371, doi:10.1039/c3cp50968k, 2013.

Theys, N., De Smedt, I., Yu, H., Danckaert, T., van Gent, J., Hörmann, C., Wagner, T., Hedelt, P., Bauer, H., Romahn, F., Pedergnana, M., Loyola, D. and Van Roozendael, M.: Sulfur dioxide retrievals from TROPOMI onboard Sentinel-5 Precursor: algorithm theoretical basis, Atmospheric Measurement Techniques, 10(1), 119–153, doi:10.5194/amt-10-119-2017, 2017.

Vandaele, A. C., Hermans, C., Simon, P. C., Carleer, M., Colin, R., Fally, S., Mérienne, M. F., Jenouvrier, A. and Coquart, B.: Measurements of the NO2 absorption cross-section from 42 000 cm−1 to 10 000 cm−1 (238–1000 nm) at 220 K and 294 K, Journal of Quantitative Spectroscopy and Radiative Transfer, 59(3–5), 171–184, doi:10.1016/S0022-4073(97)00168-4, 1998.

Veefkind, J. P., Aben, I., McMullan, K., Förster, H., de Vries, J., Otter, G., Claas, J., Eskes, H. J., de Haan, J. F., Kleipool, Q., van Weele, M., Hasekamp, O., Hoogeveen, R., Landgraf, J., Snel, R., Tol, P., Ingmann, P., Voors, R., Kruizinga, B., Vink, R., Visser, H. and Levelt, P. F.: TROPOMI on the ESA Sentinel-5 Precursor: A GMES mission for global observations of the atmospheric composition for climate, air quality and ozone layer applications, Remote Sensing of Environment, 120, 70–83, doi:10.1016/j.rse.2011.09.027, 2012.

Verhoelst, T., Compernolle, S., Pinardi, G., Lambert, J.-C., Eskes, H. J., Eichmann, K.-U., Fjæraa, A. M., Granville, J., Niemeijer, S., Cede, A., Tiefengraber, M., Hendrick, F., Pazmiño, A., Bais, A., Bazureau, A., Boersma, K. F., Bognar, K., Dehn, A., Donner, S., Elokhov, A., Gebetsberger, M., Goutail, F., Grutter de la Mora, M., Gruzdev, A., Gratsea, M., Hansen, G. H., Irie, H., Jepsen, N., Kanaya, Y., Karagkiozidis, D., Kivi, R., Kreher, K., Levelt, P. F., Liu, C., Müller, M., Navarro Comas, M., Piters, A. J. M., Pommereau, J.-P., Portafaix, T., Puentedura, O., Querel, R., Remmers, J., Richter, A., Rimmer, J., Rivera Cárdenas, C., Saavedra de Miguel, L., Sinyakov, V. P., Strong, K., Van Roozendael, M., Veefkind, J. P., Wagner,

T., Wittrock, F., Yela González, M., and Zehner, C.: Ground-based validation of the Copernicus Sentinel-5p TROPOMI NO_2 measurements with the NDACC ZSL-DOAS, MAX-DOAS and Pandonia global networks, Atmos. Meas. Tech. Discuss., https://doi.org/10.5194/amt-2020-119, in review, 2020.

Volkamer, R., Spietz, P., Burrows, J. and Platt, U.: High-resolution absorption cross-section of glyoxal in the UV–vis and IR spectral ranges, Journal of Photochemistry and Photobiology A: Chemistry, 172(1), 35–46, doi:10.1016/j.jphotochem.2004.11.011, 2005.

Wang, P., Piters, A., van Geffen, J., Tuinder, O., Stammes, P. and Kinne, S.: Shipborne MAX-DOAS measurements for validation of TROPOMI NO2 products, Atmospheric Measurement Techniques, 13(3), 1413–1426, doi:10.5194/amt-13-1413-2020, 2020.

Williams, J. E., Boersma, K. F., Le Sager, P. and Verstraeten, W. W.: The high-resolution version of TM5-MP for optimized satellite retrievals: description and validation, Geoscientific Model Development, 10(2), 721–750, doi:10.5194/gmd-10-721-2017, 2017.

Yang, K., Carn, S. A., Ge, C., Wang, J. and Dickerson, R. R.: Advancing measurements of tropospheric NO2 from space: New algorithm and first global results from OMPS, Geophysical Research Letters, 41(13), 4777–4786, doi:10.1002/2014GL060136, 2014.

Zhao, X., Griffin, D., Fioletov, V., McLinden, C., Cede, A., Tiefengraber, M., Müller, M., Bognar, K., Strong, K., Boersma, F., Eskes, H., Davies, J., Ogyu, A. and Lee, S. C.: Assessment of the quality of TROPOMI high-spatial-resolution NO2 data products, , doi:10.5194/amt-2019-416, 2019.

Zoogman, P., Liu, X., Suleiman, R. M., Pennington, W. F., Flittner, D. E., Al-Saadi, J. A., Hilton, B. B., Nicks, D. K., Newchurch, M. J., Carr, J. L., Janz, S. J., Andraschko, M. R., Arola, A., Baker, B. D., Canova, B. P., Chan Miller, C., Cohen, R. C., Davis, J. E., Dussault, M. E., Edwards, D. P., Fishman, J., Ghulam, A., González Abad, G., Grutter, M., Herman, J. R., Houck, J., Jacob, D. J., Joiner, J., Kerridge, B. J., Kim, J., Krotkov, N. A., Lamsal, L., Li, C., Lindfors, A., Martin, R. V., McElroy, C. T., McLinden, C., Natraj, V., Neil, D. O., Nowlan, C. R., O'Sullivan, E. J., Palmer, P. I., Pierce, R. B., Pippin, M. R., Saiz-Lopez, A., Spurr, R. J. D., Szykman, J. J., Torres, O., Veefkind, J. P., Veihelmann, B., Wang, H., Wang, J. and Chance, K.: Tropospheric emissions: Monitoring of pollution (TEMPO), Journal of Quantitative Spectroscopy and Radiative Transfer, 186, 17–39, doi:10.1016/j.jqsrt.2016.05.008, 2017.

Table 1: A priori input for tropospheric AMF calculations for TROPOMI and airborne TrVCs

	TROPOMI v1.2	Airborne
A priori NO_2 profile shape	TM5-MP 1° × 1° model (Williams et al., 2017)	Troposphere: 12 km NAMCMAQ (Stajner et al., 2011) Stratosphere: PRATMO Climatology (Prather, 1992; McLinden et al., 2000) bias corrected daily with TROPOMI Stratospheric Vertical Columns
Surface Reflectivity	OMI 0.5°× 0.5° 5-year climatology (Kleipool et al., 2008)	Land: MCD43A1 daily L3 500m v006 product (Lucht et al., 2000; Schaaf and Wang, 2015) averaged over the period of the campaign Water: Assumed Lambertian reflectance of at least 3% and Cox-Monk kernel
Pressure/Temperature Profiles	TM5-MP 1° × 1° model driven by the ECMWF corrected with a 3-km DEM	Troposphere: 12 km NAMCMAQ (Stajner et al., 2011) Stratosphere: 1º RAQMS (Pierce et al., 2009)
Clouds	FRESCO-S (Loyola et al., 2018)	Cloudy scenes are not included in this analysis

Table 2: Comparison of GeoTASO and GCAS

	GeoTASO	GCAS
Spectral Range	290-390nm, 415-695nm	300-490nm, 480-900nm
Spectral Resolution	0.43nm, 0.88nm	0.6nm, 2.8nm
Size/Weight	90 kgs	36 kgs
Detector dimensions	1056 spectral × 1033 spatial	1072 spectral × 1024 spatial
Integration times	250 ms	225 to 750 ms
Native spatial resolution	Approximately 250 m × 250 m	
Field of View	45 degrees	
References	Leitch et al., 2014 Nowlan et al., 2016 Judd et al., 2019	Kowalewski and Janz, 2014 Nowlan et al., 2018

Deleted: 200

Deleted: lbs

Deleted: 80

Deleted: lbs

Deleted: ¶

Table 3: GeoTASO/GCAS Flight Summary for LISTOS. Flights with shaded boxes are not considered in this analysis.

Flight	Date	Time (UTC fractional hour)	Pollution Scale (95th percentile $\times 10^{15}$ molecules cm^{-2})	% Cloudy Pixels	# Valid Pandora Coincidences	# Valid TROPOMI Coincidences	Flight pattern type (Fig. 1)
1	18 Jun. 2018	12.0-15.6					Large
2		17.0-20.7					Large
3	25 Jun. 2018	12.5-15.7	7.3	10	5	34	Small
4		16.8-20.3	7.2	5			Small
5	30 Jun. 2018	12.2-15.6	11.2	0	9	65	Small
6		16.7-20.4	13.5	1			Small
7	02 Jul. 2018	11.4-16.6	14.5	0	7	18	Small
8		17.9-21.5	18.9	0			Small
9	19 Jul. 2018	11.4-15.3	17.9	0	11	47	Large
10		16.9-20.9	32.4	0			Large
11	20 Jul. 2018	11.4-15.3	30.4	3	15	38	Large
12		17.1-21.1	16.3	5			Large
13	05 Aug. 2018	12.5-16.5	15.5	1	15	0	Large
14		17.8-22.3	10.2	5			Large
15	06 Aug. 2018	11.7-16.0	21.3	0	13	11	Large
16		17.2-21.5	16.1	5			Small
17	15 Aug. 2018	11.2-15.5	12.4	0	17	52	Large
18		17.0-21.6	9.8	5			Large
19	16 Aug. 2018	11.3-15.3	13.7	17	16	31	Small
20		17.3-21.5	9.8	2			Small
21	24 Aug. 2018	10.9-15.3	14.7	0	18	32	Large
22		16.6-21.0	37.8	4			Large
23	28 Aug. 2018	11.3-15.3	16.6	0	15	10	Small
24		16.6-20.3	16.0	2			Small
25	29 Aug. 2018	11.2-15.1	16.8	0	17	17	Small
26		16.6-20.8	14.0	3			Small
27	06 Sept. 2018	11.9-15.8	11.8	9	13	33	Small
28		17.2-21.4	12.2	5			Small
29	03 Oct. 2018	12.3-16.7					Small
30		18.2-21.8					Small
31	19 Oct. 2018	12.8-15.2					Small
32		16.8-20.3					Small

Table 4: Pandora sites and time of operation. Shaded boxes represent the months of LISTOS.

Pandora Name	Latitude, Longitude	Months with Valid Data (number of measurement days per month)									
		2018							2019		
		J	J	A	S	O	N	D	J	F	M
QueensNY	40.7361, -73.8215	5	23	27	26	27	27	25	26	26	29
BronxNY	40.8679, -73.8781	6	29	29	16	21	10	-	-	-	-
BayonneNJ	40.6703, -74.1261	-	21	31	27	26	25	25	26	24	28
FlaxPondNY	40.9635, -73.1402	2	13	28	19	5	-	-	-	-	-
WestportCT	41.1183, -73.3367	5	19	29	25	27	24	26	23	5	22
NewHavenCT	41.3014, -72.9029	6	30	29	19	19	14	24	15	-	-
RutgersNJ	40.4622, -74.4294	2	30	30	21	27	22	25	21	5	21
MadisonCT	41.2568, -72.5533	7	13	-	-	-	-	-	-	-	-
BranfordCT	41.2420, -72.7604	-	9	30	4	-	-	-	-	-	-

Table 5: Statistics for TROPOMI and airborne comparisons with the coincidence criteria of CRF < 50% and aircraft sampled within ± 30 minutes of the S5P overpass with different a priori profiles and indication of whether the Δ_{CS} threshold is applied.

TROPMI Dataset	Δ_{CS} < 50hPa	RMA Fit	r^2	Median Percent Difference	N
Standard Slant Column	No	y=0.58x+1.5×10^{15}	0.95	-12%	621
	Yes	y=0.59x+1.5×10^{15}	0.96	-13%	388
Standard TrVC	No	y=0.71x+0.9×10^{15}	0.90	-11%	621
	Yes	y=0.68x+0.6×10^{15}	0.96	-19%	388
NAMCMAQ TrVC	No	y=0.84x+1.0×10^{15}	0.83	4%	621
	Yes	y=0.77x+0.7×10^{15}	0.95	-7%	388

Deleted: --

Deleted: --

Table 6: Statistics between Pandora and TROPOMI by site for the LISTOS period as well as extended to 19 March 2019

	LISTOS Only (June-September 2018)					Valid data from June 2018-March 2019				
Site	RMA Fit	r^2	Median % Difference	Median Column Difference	N	RMA Fit	r^2	Median % Difference	Median Column Difference	N
QueensNY	Y=0.77x+0.6×10^{15}	0.87	-9%	-0.5×10^{15}	22	Y=0.63x+1.3×10^{15}	0.76	-23%	-2.1×10^{15}	68
BronxNY	Y=0.81x+0.03×10^{15}	0.90	-15%	-1.1×10^{15}	20	Y=0.73x+0.5×10^{15}	0.87	-15%	-1.1×10^{15}	33
BayonneNJ	Y=0.84x-2.1×10^{15}	0.87	-38%	-4.1×10^{15}	9	Y=0.74x-1.8×10^{15}	0.88	-41%	-5.3×10^{15}	45
WestportCT	Y=0.49x+1.1×10^{15}	0.50	-19%	-0.6×10^{15}	21	Y=0.68x+0.4×10^{15}	0.95	-21%	-0.9×10^{15}	49
RutgersNJ	Y=0.63x+0.4×10^{15}	0.69	-26%	-0.9×10^{15}	6	Y=0.76x-0.1×10^{15}	0.95	-24%	-1.4×10^{15}	33
FlaxPondNY	Y=0.53x+0.4×10^{15}	0.59	-37%	-1.7×10^{15}	23	Y=0.53x+0.5×10^{15}	0.60	-37%	-1.4×10^{15}	25
NewHavenCT	Y=0.52x-0.5×10^{15}	0.29	-52%	-2.7×10^{15}	25	Y=0.70x-1.3×10^{15}	0.71	-50%	-2.7×10^{15}	47
BranfordCT	Y=1.22x-2.7×10^{15}	0.31	-46%	-1.9×10^{15}	22	Y=1.2x-2.7×10^{15}	0.31	-46%	-1.9×10^{15}	22
MadisonCT	Y=1.94x-2.7×10^{15}	0.12	-24%	-0.6×10^{15}	8	Y=2.4x-3.9×10^{15}	0.02	-24%	-0.7×10^{15}	11

Table 7: Summary statistics for Pandora and TROPOMI over the LISTOS time period and extended to 19 March 2019 with different a priori profiles and indication of whether the ΔCS threshold is applied.

Time Period	Location	TROPMI Dataset	Δ_{CS} < 50hPa	RMA Fit	r^2	Median Percent Difference	N
LISTOS Only	All Sites	Standard	No	$y=0.82x-0.6\times10^{15}$	0.79	-30%	294
			Yes	$y=0.80x-0.7\times10^{15}$	0.84	-33%	156
		NAMCMAQ	No	$y=1.05x-0.7\times10^{15}$	0.77	-9%	294
			Yes	$y=0.82x-0.2\times10^{15}$	0.80	-19%	156
LISTOS Only	RutgersNJ	Standard	No	$y=0.78x-0.5\times10^{15}$	0.79	-17%	132
	BayonneNJ		Yes	$y=0.76x+0.1\times10^{15}$	0.88	-19%	58
26 June 2018 — 19 March 2019	QueensNY		No	$y=0.74x+0.2\times10^{15}$	0.82	-21%	373
	WestportCT		Yes	$y=0.78x-0.3\times10^{15}$	0.87	-27%	195

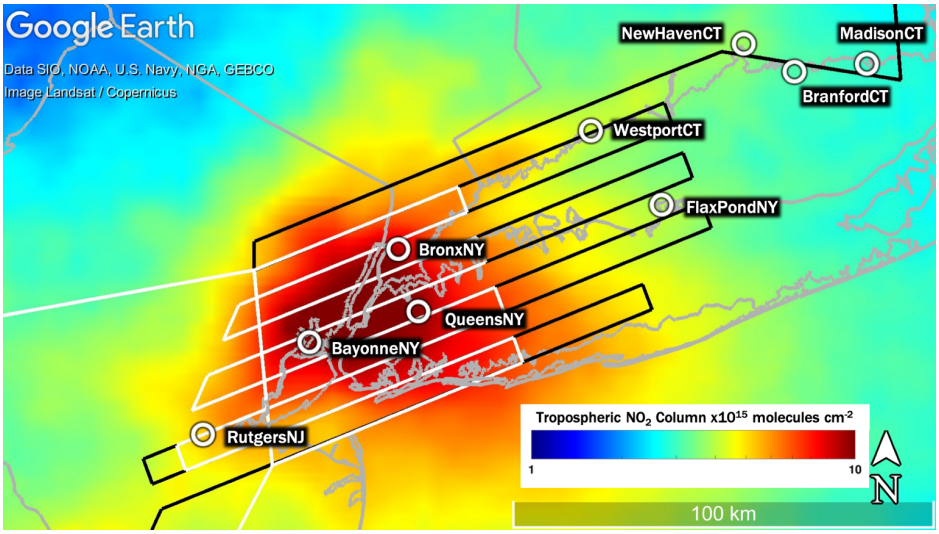

Figure 1: Map showing the annual average TROPOMI tropospheric NO_2 columns between April 2018-March 2019. Overlaid circles show the locations of the nine Pandora spectrometers considered in this analysis. Table 4 shows when each of these instruments operated. The black and white lines represent the two types of flight plans flown by the airborne spectrometers (large in black and small in white). This map was created in © Google Earth Pro.

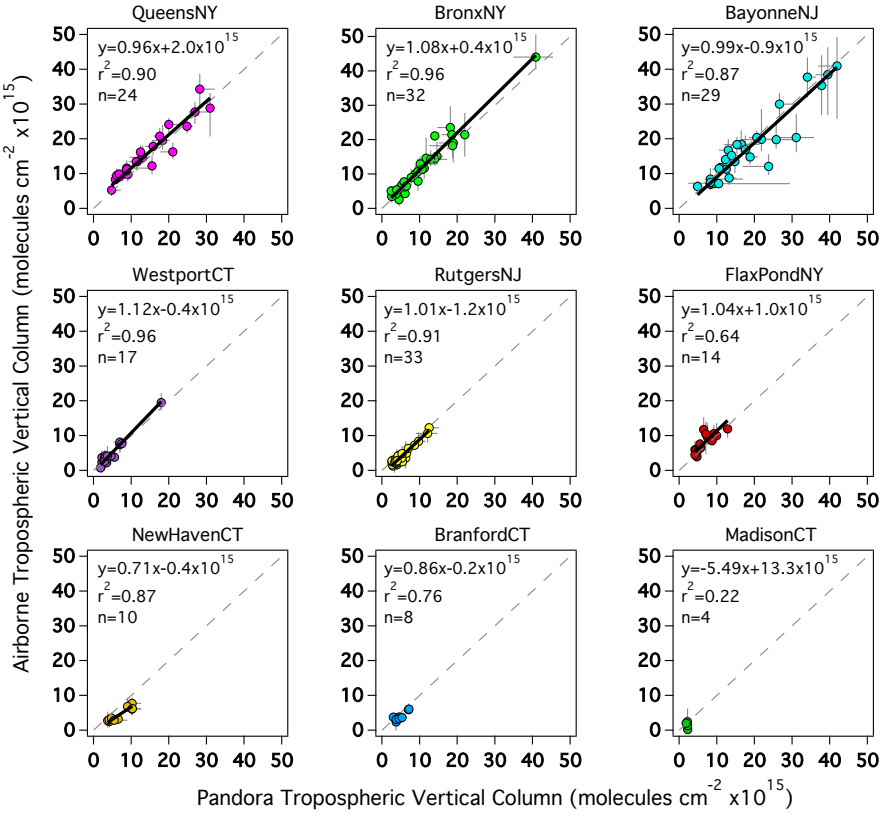

Figure 2: Scatter plots of the temporally closest Pandora TrVC to the aircraft overpass (± min/max observation within a ± 5-minute window from the aircraft overpass) vs. median airborne TrVC within a 750m radius of Pandora (±10th-90th percentile) with labeled statistics. 1:1 line is indicated with the grey dashed line. The solid black lines indicate the RMA linear regression for sites with r^2 greater than 0.5.

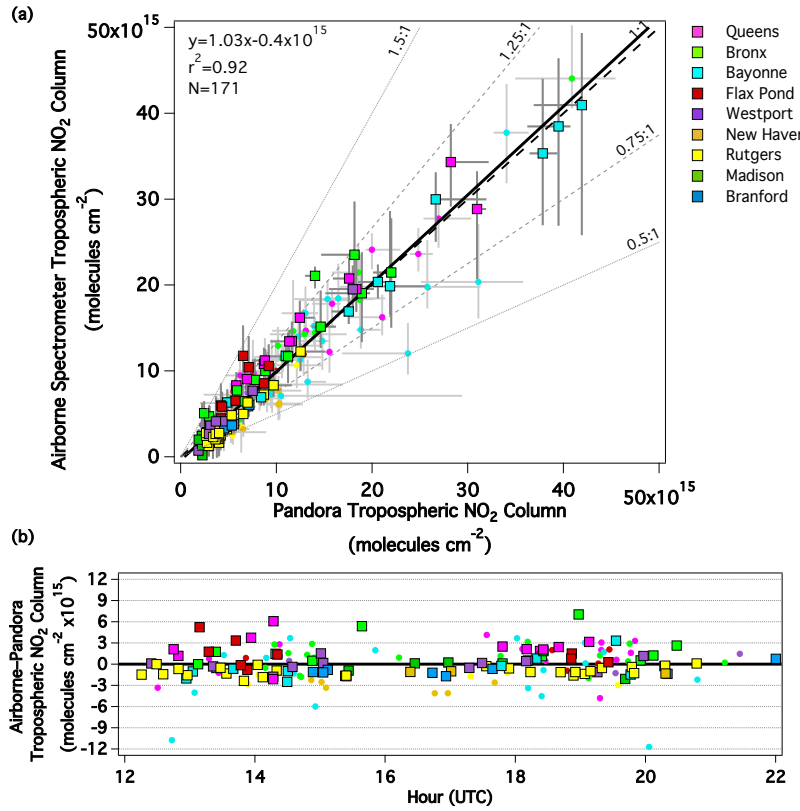

Figure 3: (a) Scatter plot showing the temporally closest Pandora TrVC to the aircraft overpass (± min/max observation within a ± 5-minute window from the aircraft overpass) vs. the median airborne TrVC (±10th-90th percentile) within a 750 m radius of the Pandora site. The thick solid black line represents the RMA linear regression. Each point is colored by Pandora location where the outlined squares are points where Pandora TrVCs do not vary more than 30% within a ± 15-minute window from the aircraft overpass, whereas the circles indicate times where Pandora TrVCs do vary more than 30%. (b) The difference between airborne and Pandora tropospheric NO_2 columns vs. time of day in hours (UTC) colored similarly to (a).

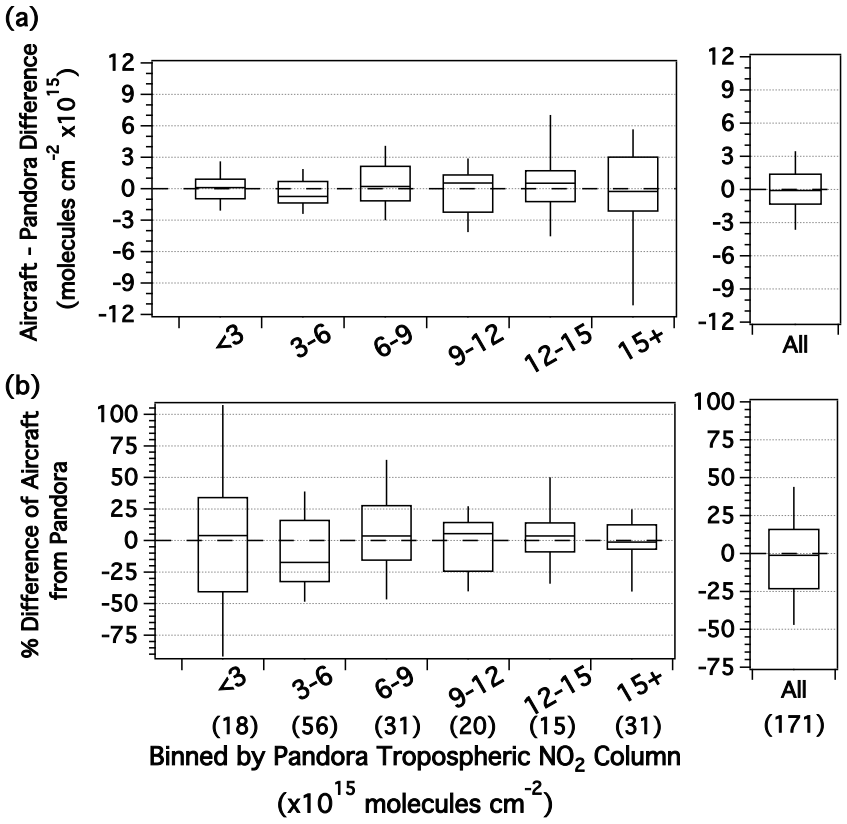

Figure 4: Box plots (95-75-50-25-5) showing the airborne column (a) column difference and (b) percent difference from Pandora binned at the labeled thresholds (×10^{15}) as well as all data points (right). The number of points in each bin are indicated by the numbers in parentheses above the x-axis label.

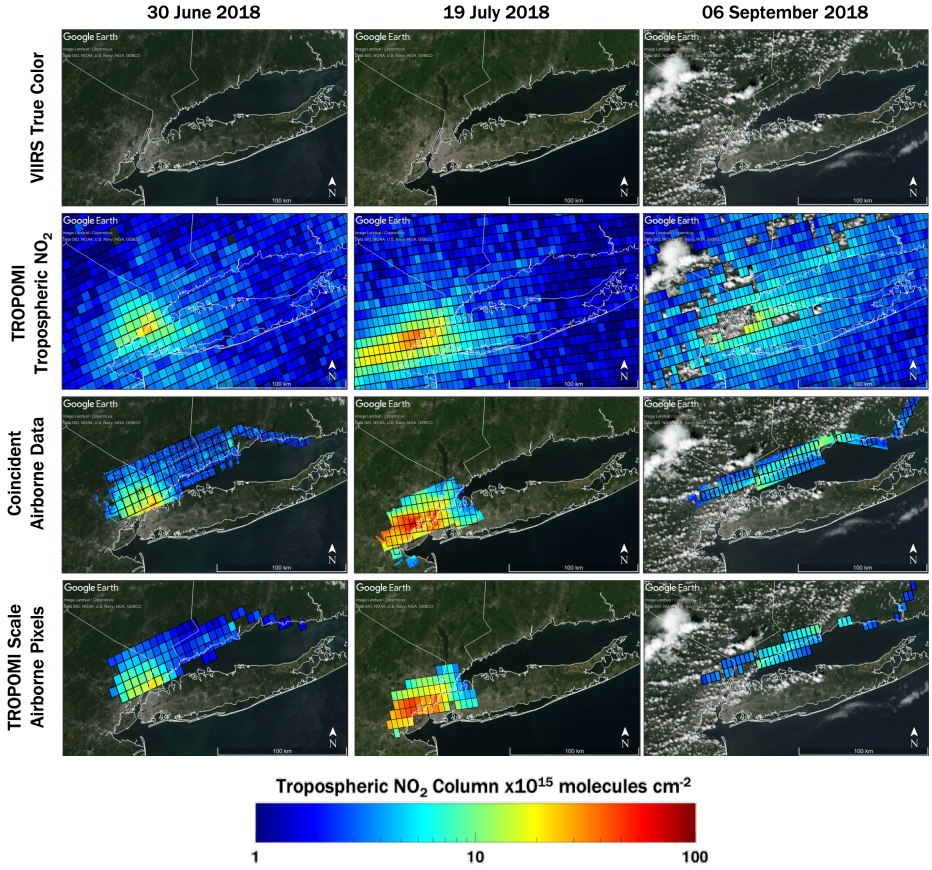

Figure 5: Maps demonstrating how airborne data is matched to TROPOMI for 3 out of 15 example overpasses: (top) VIIRS true color imagery (source: https://worldview.earthdata.nasa.gov/: last accessed 18 April 2020), (second row) overlaid TROPOMI TrVCs where CRFs < 50%, (third row) overlaid airborne data collected within ± 30 minutes of the TROPOMI overpass with outlined TROPOMI pixels with CRFs < 50% and area mapped by aircraft > 75%, (bottom) airborne NO_2 columns data scaled to the TROPOMI pixel. All maps were created in © Google Earth Pro.

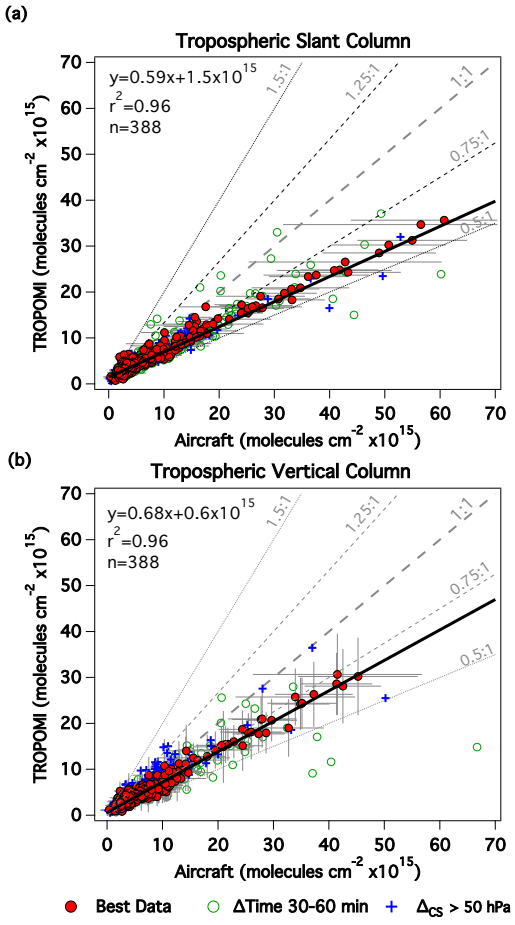

Figure 6: Scatter plots of airborne data gridded and scaled up to the TROPOMI pixel footprint vs. TROPOMI NO_2 tropospheric (a) slant column and (b) vertical column that are at least 75% mapped with a CRF < 50 % within ± 30 min of the TROPOMI overpass in red circles (open green circles show points when the time window is expanded to ± 60 min and blue crosses symbolize points where Δ_{CS} > 50 hPa). The horizontal bars indicate the sub-pixel heterogeneity measured by the aircraft quantified as the standard deviation of aircraft slant columns over that pixel and vertical bars in (b) show the reported precision of the TROPOMI TrVC (the precision of the tropospheric slant columns in panel a are not large enough to be visible in this figure but the average is $5x10^{14}$ molecules cm^{-2} with a standard deviation of $7x10^{13}$ molecules cm^{-2}).

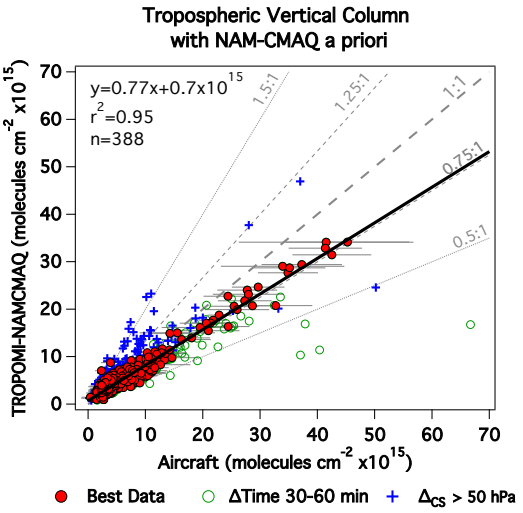

Figure 7: Scatter plots of airborne data gridded and scaled up to the TROPOMI pixel footprint vs. TROPOMI-NAMCMAQ NO_2 TrVCs that are at least 75% mapped with a CRF < 50 % within ± 30 min of the TROPOMI overpass in red circles (open green circles show points when the time window is expanded to ± 60 min and blue crosses symbolize points where Δ_{CS} > 50 hPA). The horizontal bars indicate the sub-pixel heterogeneity measured by the aircraft quantified as the standard deviation of aircraft vertical columns over that TROPOMI pixel.

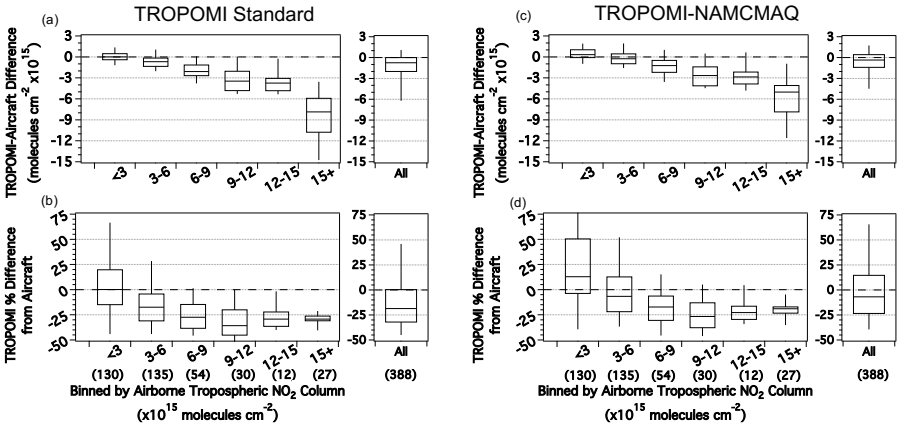

Figure 8: Box plots (95-75-50-25-5) showing the TROPOMI TrVC (a) column difference and (b) percent difference from airborne TrVCs binned at the labeled thresholds (×10^{15}) as well as for the total dataset (right), along with the equivalent box plots for TROPOMI-NAMCMAQ in (c) and (d). The number of points in each bin are indicated by the numbers in parentheses above the x-axis label.

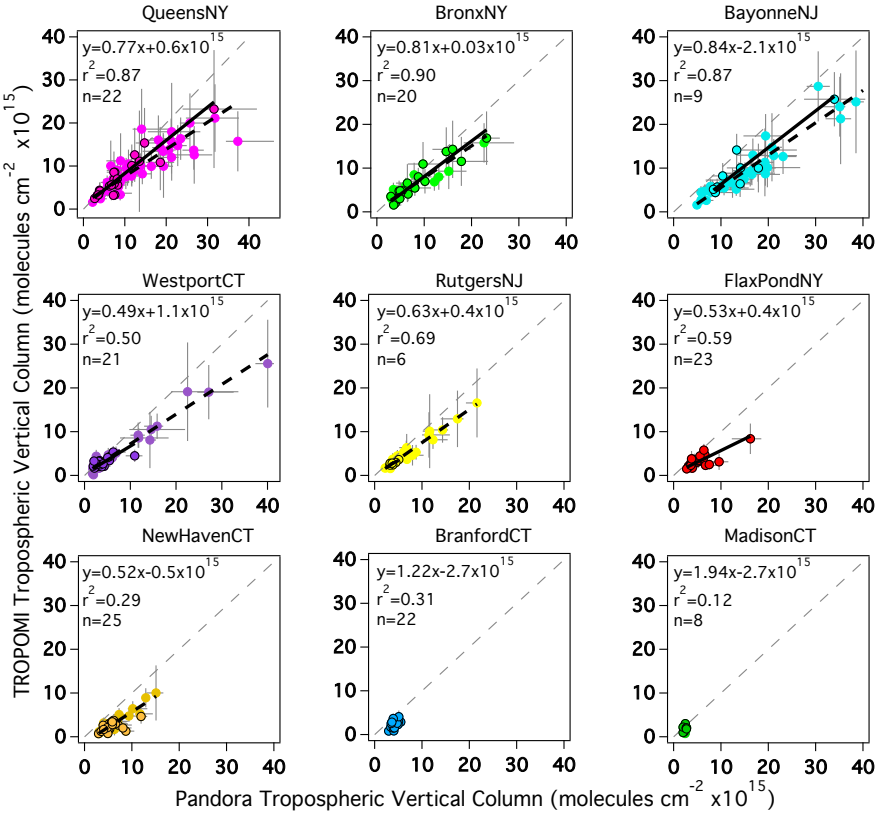

Figure 9: Scatter plots of the median Pandora TrVC within ± 30 min of the S5P overpass vs. TROPOMI TrVC for all coincidences with CRF < 50%, Δ_{CS} < 50 hPa between June 25th 2018 and 19 March 2019 at each individual site. Coincidences during the LISTOS intensive period (through the end of September 2018) are outlined in black. Vertical bars indicate the reported precision of TROPOMI TrVCs and the horizontal bars are the 10th-90th percentile of Pandora TrVCs within ± 30 min of the S5P overpass. 1:1 line is indicated with the grey dashed line. Statistics are summarized in Table 6 but the RMA regression lines are shown for datasets with r^2 greater than 0.5 (solid black line is for the LISTOS timeframe and dashed black line is all data).

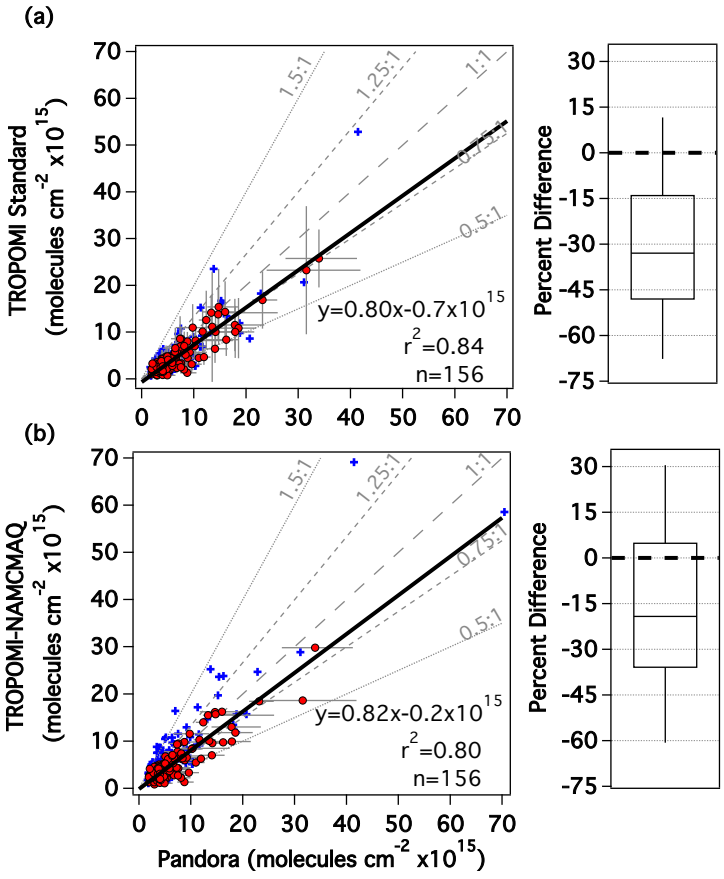

Figure 10: Scatter plot showing coincident (a) TROPOMI Standard TrVCs and (b) TROPOMI-NAMCMAQ TrVCs with CRF < 50% vs. median Pandora NO_2 TrVC over a ± 30-minute temporal window during the LISTOS intensive period. Red points have a Δ_{CS} < 50 hPa, whereas blue crosses have a Δ_{CS} > 50 hPa. The horizontal bars represent the 10th-90th percentile of Pandora data within the ±30 min temporal window. The vertical bars in (a) represent the reported precision of TROPOMI Standard. The thick solid black line represents the RMA linear regression applied to the red data points. The box plots (95-75-50-25-5) show the TROPOMI TrVC percent difference from Pandora for the red data points to the right of each scatter plot.

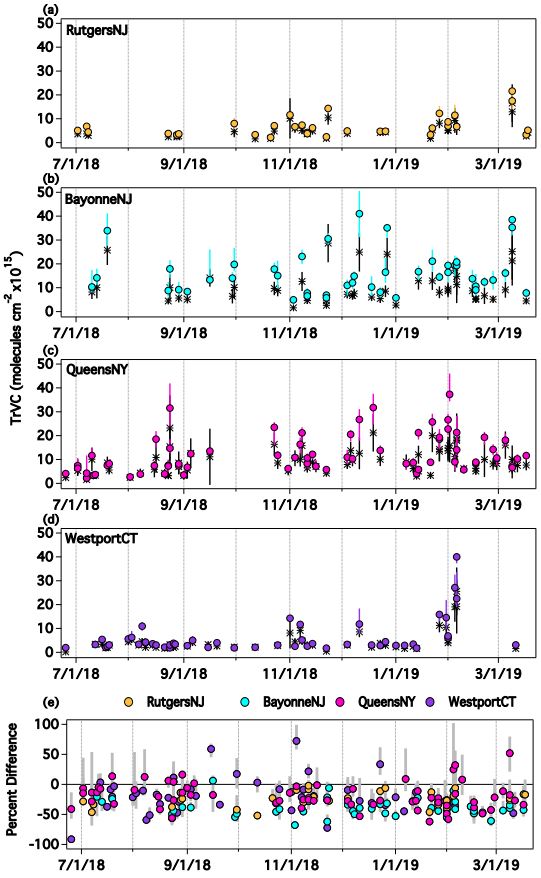

Figure 11: Time series of Pandora and TROPOMI Standard TrVCs from 25 June 2018 through 19 March 2019. Circles represent the Pandora data ± 10th-90th percentile in the ± 30-minute window and the stars indicated the TROPOMI TrVC ± the reported precision at (a) RutgersNJ, (b) BayonneNJ, (c) QueensNY, and (d) WestportCT. The percent difference of the TROPOMI Standard TrVC from Pandora colored by site is shown in (e) and the grey bars indicate the 10th-90th percentile of the column difference of TROPOMI TrVC from the sub-temporal Pandora data.

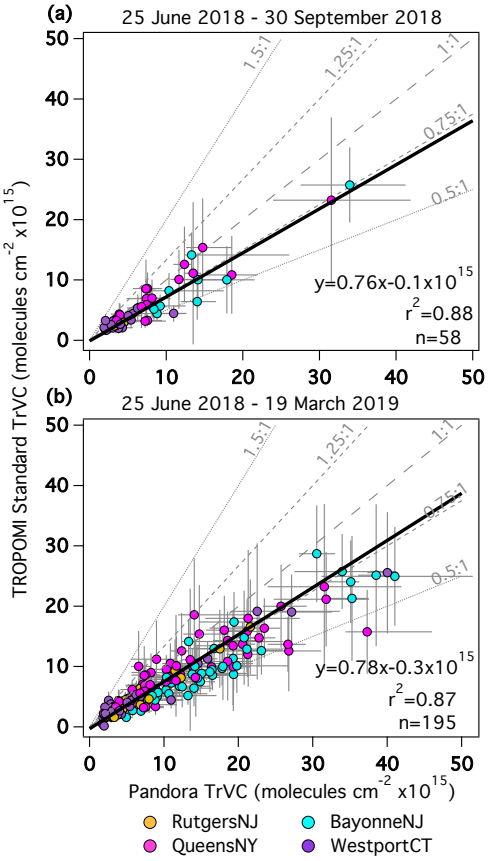

Figure 12: TROPOMI Standard vs Pandora TrVCs colored by site during (a) the LISTOS intensive period for the four locations with extended measurements in time (RutgersNJ, BayonneNJ, QueensNY, WestportCT) followed by (b) coincidences extending from 25 June 2018 – 19 March 2019 at the same four sites. The horizontal bars represent the 10th-90th percentile of Pandora data within the ±30 min temporal window. The vertical bars represent the reported precision of TROPOMI. Each point is colored by Pandora location.

Deleted: and

Supplement to Evaluating Sentinel-5P TROPOMI tropospheric NO_2 column densities with airborne and Pandora spectrometers near New York City and Long Island Sound

S1. Sensitivity of Airborne/Pandora comparisons to coincidence criteria

Table S1 shows the sensitivity of the aircraft-Pandora aggregate linear regression to the coincidence criteria. Coincidence criteria varied to include the radial distance from the Pandora location, Pandora viewing azimuth, temporal window of Pandora data, temporal averaging and filtering of Pandora data, and the range in the S5P TROPOMI overpass time.

Table S1: Airborne v. Pandora column statistics based on temporal and spatial coincidence criteria.

Coincidence Criteria			Statistics			
Row	**Temporal Criteria**	**Spatial Aircraft Criteria**	**Slope**	**Offset (molecules cm^{-2})**	**r^2**	**N**
A	Temporally closest Pandora coincidence	Median 250 m radius	1.13±0.03	$-0.8\times10^{15}\pm 0.3\times10^{15}$	0.91	129
B		Median 750 m radius	1.03±0.03	$-0.4\times10^{15}\pm 0.2\times10^{15}$	0.92	171
C		Median 1.5 km radius	0.98±0.04	$-0.1\times10^{15}\pm 0.3\times10^{15}$	0.89	177
D		Median 750 m radius (±45 degree sector)	1.07±0.03	$-0.6\times10^{15}\pm 0.3\times10^{15}$	0.92	169
E		Median 750 m radius (±22.5 degree sector)	1.08±0.03	$-0.7\times10^{15}\pm 0.3\times10^{15}$	0.92	167
F	Pandora Median ±5 min	Median 750m radius	1.03±0.03	$-0.4\times10^{15}\pm 0.3\times10^{15}$	0.91	171
G	Pandora Median ±15 min		1.03±0.03	$0.3\times10^{15}\pm 0.2\times10^{15}$	0.92	176
H	Temporally closest Pandora coincidence but excluding Temporally variable data		1.05±0.04	$-0.3\times10^{15}\pm 0.3\times10^{15}$	0.96	97
I	Coincidences during the TROPOMI Overpass Window (16.7-19.0 UTC)		1.14±0.03	$-1.1\ x10^{15}\pm 0.3\times10^{15}$	0.94	47

Row B presents results with the baseline criteria used in this analysis: the instantaneous Pandora observation closest in time to the aircraft overflight within ±5 minutes of the overflight and the median of the airborne data within a 750 m radius of the sites. These were the same criteria implemented in Judd et al. (2019). This is the dataset that results in the highest r^2 except for the subsets based on temporal variability and TROPOMI temporal window (Rows H and I)

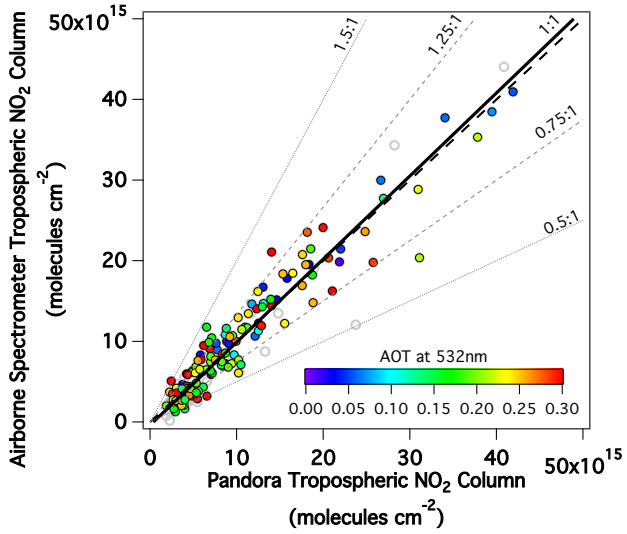

Figure S1: Scatter plot showing the temporally closest Pandora TrVC to the aircraft overpass vs. the median airborne TrVC within a 750 m radius of the Pandora site (same as Figure 3) colored by AOT measured by the HALO Lidar at 532 nm. Open grey circles are coincidences that occurred without HALO data.

Commented [JLM(1)]: I noticed that the color bar in this figure was reversed. This is fixed now.

Figure S1 shows the impact of aerosol loading on the Pandora and airborne TrVC comparison as aerosols are not included as a priori input in the airborne AMF calculation. Over 90% of these coincidences have an AOT at 532 nm < 0.3, two coincidences are above 0.5 with a max of 0.7. There does not appear to be any relation to aerosol loading in the Pandora/aircraft comparison, though future work could calculate AMFs explicitly accounting for aerosol profile properties and loading for times when HALO data is available.

Formatted: Font color: Black, English (US)

S2. Sensitivity of Airborne/TROPOMI comparisons to coincidence criteria

Table S2 shows the sensitivity of coincidence criteria on airborne TrVC comparisons to TROPOMI. Coincidence criteria varied to include the temporal window in which aircraft data is extracted from the TROPOMI overpass time, the percentage of the TROPOMI pixel that is mapped by the aircraft within that temporal window, cloud radiative fraction (CRF), and Δ_{CS}, which is defined as the difference in surface and cloud pressures in the TROPOMI product file, discussed in Sect 4.1 in the main manuscript. The applied coincidence criteria in this work is shown in Row M; these criteria are airborne data collected within ± 30 min of the TROPOMI overpass for pixels that are at least 75% mapped with CRFs less than 50% and $\Delta_{CS} < 50$ hPa. This set of criteria resulted in nearly the highest r^2, where the exception was for all the same critieria but for CRFs confined to less than 20-30%. However, the tradeoff for allowing CRFs up to 50% results in more data points included in the analysis with no change in the slope.

Table S2: Airborne vs. TROPOMI statistics for varying temporal windows, mapped percentage by the aircraft of TROPOMI pixels, Cloud Radiative Fraction (CRF), Δ_{CS} filter.

Row	Temporal Window	% Mapped	CRF	$\Delta_{CS} < 50$ hPa Filter	Slope	Intercept $\times 10^{15}$	r^2	N
A	**± 60 min**	**75%**			0.67±0.03	1.0±0.2	0.80	1068
B		**75%**			0.71±0.02	0.9±0.1	0.90	621
C	**± 30 min**	**50%**	**< 50%**	No	0.72±0.02	1.0±0.1	0.89	814
D		**25%**			0.75±0.03	1.1±0.1	0.83	1004
E	**± 15 min**	**75%**			0.72±0.03	0.8±0.2	0.93	285
F			**< 50%**		0.71±0.02	0.9±0.1	0.90	621
G			**< 30%**	No	0.70±0.03	0.9±0.1	0.94	452
H			**< 20%**		0.70±0.02	0.8±0.1	0.96	290
I		**75%**	**< 10%**		0.67±0.02	0.9±0.1	0.95	165
J	**± 30 min**		**< 50%**		0.68±0.01	0.6±0.1	0.96	388
K			**< 30%**		0.68±0.01	0.8±0.1	0.97	313
L			**< 20%**	Yes	0.68±0.01	0.8±0.1	0.97	202
M			**< 10%**		0.66±0.02	0.9±0.1	0.96	118
N		**50%**	**<50%**		0.70±0.01	0.7±0.1	0.93	487
O		**25%**			0.73±0.03	0.9±0.1	0.86	584

S3. Case Study Illustrating Sensitivity to Cloud Pressure for Δ_{CS} threshold

When comparing the aircraft data to TROPOMI, two outliers (apparent in Figures 6 and 7 in the main manuscript) extend well above the main population of data. These points occured on July 19th, 2018, for TROPOMI pixels viewing the urban areas of eastern New Jersey just across the river from Manhattan Island NYC (red outlined points in Figure S2). VIIRS true-color imagery (Figure 5 in the main manuscript) shows that there are zero clouds in the domain. Even without the presence of clouds, TROPOMI CRFs extend up to 33% over the LISTOS domain demonstrating how limiting CRFs to those below 20% only would exclude many comparisons over the bright urban surfaces in this domain.

For the outlier pixels, TROPOMI retrieves a 19 and 23% CRF, similar to nearby pixels which do not result in outliers. The difference lies within the retrieved cloud pressure in relation to the surface pressure. In the case of the two outliers, the cloud pressure is above 800 hPa, which is reflected in the loss of sensitivity as seen in the box AMF profiles in grey in Figure S2. The impact of aerosols has been ruled out for this instance as the airborne HALO instrument retrieved AOT at 532nm of 0.04. The other coincidences on this day have a median cloud pressure of 984 hPa with a standard deviation of 29 hPa (median surface pressure is 1016 hPa). The reported uncertainty in cloud pressure is 50 hPa in van Geffen et al., (2019).

Adjusting box AMFs to remove the estimated loss of sensitivity below the retrieved cloud level (red line in profiles in Figure S2) and recalculating tropospheric AMF results in an increase in AMF (changing from 0.61 and 0.68 to 1.00 and 1.09, respectively, using the 12 km NAMCMAQ a priori profile) which brings these two outliers into agreement with the rest of the data population (within the distribution of the red circles in Figure 7).

Deleted: of

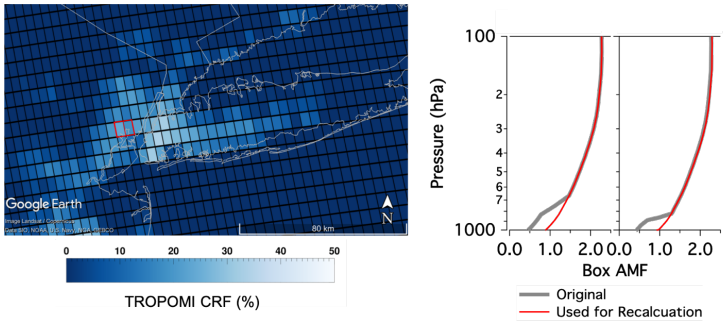

Figure S2: Map showing TROPOMI's CRF retrieved during the 19 July 2018 S5P overpass and original BoxAMFs (grey line) for the pixels outlined in red the map along with a second BoxAMF that is used to recalculate the TROPOMI tropospheric AMF with the removal of the impact of clouds

S4. Sensitivity of TROPOMI/Pandora comparisons to coincidence criteria

Table S3 shows the sensitivity of coincidence criteria on Pandora TrVC comparisons to TROPOMI. Coincidence criteria varied to include the temporal window in which Pandora data is analyzed from the TROPOMI overpass time, CRF, and the Δ_{CS} threshold discussed in Sect 4.1 in the main manuscript. The applied coincidence criteria are shown in Row C and Row J (repeated for ease of comparison in the table); these are the median Pandora TrVC within a ± 30 min window from the TROPOMI overpass with TROPOMI CRFs less than 50% and Δ_{CS} less than 50 hPA.

Comparison of Rows A, B, and D to Row C shows the sensitivity to length of time over which the median is calculated from Pandora data. Additionally, comparison of Row E to Rows A-D shows the effect of using the instantaneous Pandora observation closest in time to the TROPOMI overpass versus temporal averaging of the Pandora data. As the temporal window gets smaller, the slope decreases likely due to spatial heteorgeneity in the TROPOMI sub-pixel area. The r^2 does not change when the temporal window is extended to ± 60 minutes, but ± 30 minutes is consistent with the airborne column comparisons which showed the effect of temporal mismatches beyond the ± 30 minute window. Additionally, comparing Rows F-I to Rows J-M shows the impact of applying the Δ_{CS} threshold. There is clear improvement in r^2 when applying the Δ_{CS} criterion.

Recent studies using Pandora data to evaluate TROPOMI NO_2 products have used different coincidence criteria in terms of the temporal window and statistics applied to Pandora data. Griffin et al. (2019) averaged Pandora data within ± 30 min window of the S5P overpass, similar to the current methodology but instead here the median is used to limit possible influence of isolated small-scale plumes that TROPOMI is likely not sensitive to. Ialongo et al. (2020) and Zhao et al. (2019) used a smaller temporal window of ± 10 minutes, though they used the average and closest coincidence, respectively. Unlike in airborne-Pandora comparisons, only considering Pandora coincidences where its TrVC does not vary more than 30% within a ± 30 min window does not improve r^2, but does show an increase in slope.

Table S3 TROPOMI v. Pandora column statistics based on coincidence criteria for the LISTOS time period

Coincidence Criteria			Statistics			
Row	**Temporal Window for Pandora Median**	**Cloud Criteria**	**Slope**	**Offset ($\times 10^{15}$ molecules cm^{-2})**	**r^2**	**N**
A	± 90 min	Δ_{CS} < 50 hPa + CRF < 50%	0.85±0.05	-0.9±0.3	0.83	157
B	± 60 min		0.82±0.04	-0.8±0.2	0.84	156
C	± 30 min		0.80±0.04	-0.7±0.2	0.84	156
D	± 15 min		0.75±0.04	-0.5±0.2	0.82	151
E	Closest Coincidence		0.73±0.04	-0.4±0.2	0.82	151
F	± 30 min	CRF<50%	0.82±0.12	-0.6±0.6	0.79	294
G		CRF<30%	0.91±0.11	-1.2±0.4	0.72	186
H		CRF<20%	0.85±0.09	-0.9±0.3	0.77	122
I		CRF<10%	0.91±NaN	-1.0±0.6	0.49	65
J		Δ_{CS} < 50 hPa + CRF < 50%	0.80±0.04	-0.7±0.2	0.84	156
K		Δ_{CS} < 50 hPa + CRF < 30%	0.82±0.06	-0.9±0.2	0.78	131
L		Δ_{CS} < 50 hPa + CRF < 20%	0.81±0.06	-0.8±0.2	0.83	90
M		Δ_{CS} < 50 hPa + CRF < 10%	1.01±0.01	-1.3±0.5	0.68	47
N	± 30 min, but excluding data Temporally variable data	Δ_{CS} < 50 hPa + CRF < 50%	0.86±0.09	-0.7±0.3	0.75	75

References

van Geffen, J., Eskes, H., Boersma, F., Maasakkers, J. D. and Veefkind, J. P.: TROPOMI ATBD of the total and tropospheric NO2 data products. http://www.tropomi.eu/sites/default/files/files/publicS5P-KNMI-L2-0005-RP-ATBD_NO2_data_products-20190206_v140.pdf (Accessed 14 April 2020), 2019.

Griffin, D., Zhao, X., McLinden, C. A., Boersma, F., Bourassa, A., Dammers, E., Degenstein, D., Eskes, H., Fehr, L., Fioletov, V., Hayden, K., Kharol, S. K., Li, S.-M., Makar, P., Martin, R. V., Mihele, C., Mittermeier, R. L., Krotkov, N., Sneep, M., Lamsal, L. N., Linden, M. ter, Geffen, J. van, Veefkind, P. and Wolde, M.: High-Resolution Mapping of Nitrogen Dioxide With TROPOMI: First Results and Validation Over the Canadian Oil Sands, Geophysical Research Letters, 46(2), 1049–1060, doi:10.1029/2018GL081095, 2019.

Ialongo, I., Virta, H., Eskes, H., Hovila, J. and Douros, J.: Comparison of TROPOMI/Sentinel-5 Precursor NO2 observations with ground-based measurements in Helsinki, Atmospheric Measurement Techniques, 13(1), 205–218, doi:10.5194/amt-13-205-2020, 2020.

Judd, L. M., Al-Saadi, J. A., Janz, S. J., Kowalewski, M. G., Pierce, R. B., Szykman, J. J., Valin, L. C., Swap, R., Cede, A., Mueller, M., Tiefengraber, M., Abuhassan, N. and Williams, D.: Evaluating the impact of spatial resolution on tropospheric NO2 column comparisons within urban areas using high-resolution airborne data, Atmospheric Measurement Techniques, 12(11), 6091–6111, doi:https://doi.org/10.5194/amt-12-6091-2019, 2019.

Zhao, X., Griffin, D., Fioletov, V., McLinden, C., Cede, A., Tiefengraber, M., Müller, M., Bognar, K., Strong, K., Boersma, F., Eskes, H., Davies, J., Ogyu, A. and Lee, S. C.: Assessment of the quality of TROPOMI high-spatial-resolution NO2 data products, , doi:10.5194/amt-2019-416, 2019.